European Journal of Mechanics / A Solids 104 (2024) 105040

Contents lists available at ScienceDirect

European Journal of Mechanics / A Solids

journal homepage: www.elsevier.com/locate/ejmsol

Energy approach to the selection of deformation pattern and active slip systems in single crystals

H. Petryk *, M. Kursa

Institute of Fundamental Technological Research, Polish Academy of Sciences, Pawińskiego 5B, 02-106 Warsaw, Poland

ARTICLE INFO

This paper is dedicated to Professor Viggo Tvergaard on the occasion of his 80th birthday.

Keywords:
Solids
Plasticity
Crystal plasticity
Material stability
Slip-system selection
Energy minimization
Quasi-minimization
Time integration
Implicit
Channel-die
Deformation band

ABSTRACT

The recently introduced quasi-extremal energy principle for incremental non-potential problems in rate-independent plasticity is applied to select the deformation pattern and active slip systems in single crystals. The standard crystal plasticity framework with a non-symmetric slip-system interaction matrix at finite deformation is used. The incremental work criterion for the formation of deformation bands is combined with the quasi-extremal energy principle for determining the active slip systems and slip increments in the bands. In this way, the incremental energy minimization approach has been extended to the non-potential problem of deformation banding in metal single crystals. It is shown that fulfilment of the mathematical criterion for incipient deformation banding in a homogeneous crystal in the multiple-slip case under certain conditions requires non-positive determinant of the hardening moduli matrix. Numerical examples of energetically preferable patterns of deformation bands are presented for Cu and Ni single crystals.

1. Introduction

Metal single crystals plastically deformed by multiple slip tend to form deformation patterns, with distinct sets of slip systems being activated in different subregions. A prominent example is the development of deformation bands with alternating lattice orientation that cover the entire crystal domain (grain). This is a different phenomenon than the more frequently analysed formation of strongly localized slip bands or shear bands that span over multiple grains, which is not examined here. This article presents the energy-based approach to the phenomenon of spontaneous deformation patterning, using the classical constitutive formulation (Hill and Rice, 1972) of the rate-independent incremental plasticity of single crystals with a generally *non-symmetric* constitutive matrix describing the slip-system interaction. The slip-systems interaction matrix defines, in a given material state, a linear relationship between slip rates and yield function rates for all slip systems, and the familiar hardening moduli matrix is part of it. The inherent non-uniqueness of the single crystal response, both with respect to the active slip-system set and the non-uniform deformation pattern, is a significant problem to overcome.

The ambiguity in the selection of active slip systems has been a major difficulty in the algorithmic treatment of rate-independent plasticity of single crystals for decades since the seminal work by Taylor (1938b), see the recent related literature (e.g., Prüger and Kiefer, 2020; Scheunemann et al., 2020; Zhang et al., 2021) and references therein. In this paper, the energy approach to the selection of active slip-systems in single crystals, presented in the recent work (Petryk and Kursa, 2022), is extended to the simultaneous selection of the non-uniform deformation pattern that results from the formation of deformation bands.

The phenomenon of deformation banding in single crystals has been observed experimentally for a long time, see an overview by Kuhlmann-Wilsdorf (1999). It corresponds to the bands of rotated lattice orientations, observed in X-ray or EBSD (electron backscatter diffraction) measurements, (e.g., Barrett and Levenson, 1939; Honeycombe, 1951; Butler et al., 2002; Dmitrieva et al., 2009), of an alternating pattern of slip-plane traces, (e.g., Lee and Duggan, 1993; Basson and Driver, 2000; Wert et al., 2003), or of misoriented domains separated by roughly parallel dense dislocation walls observed by electron microscopy, (e.g., Bay et al., 1989; Huang and Hansen, 1997; Hughes et al., 1997; Huang and Winther, 2007). Generally, each deformation band within a grain deforms differently than the grain on average. The phenomenon of deformation banding was characterized by Kuhlmann-Wilsdorf et al. (1999) as 'a potentially most valuable tool for the understanding of the mechanism of plastic deformation'.

* Corresponding author.
E-mail addresses: hpetryk@ippt.pan.pl (H. Petryk), mkursa@ippt.pan.pl (M. Kursa).

https://doi.org/10.1016/j.euromechsol.2023.105040
Received 16 January 2023; Received in revised form 22 April 2023; Accepted 30 May 2023
Available online 3 June 2023

As explained in earlier works (Chin and Wonsiewicz, 1969; Bay et al., 1989, 1992; Lee and Duggan, 1993; Lee et al., 1993), plastic flow is easier when some slip systems are active in one family of bands and other slip systems are active in another family of bands. In this case, the overall cross-hardening of active slip systems is reduced, resulting in a lower total plastic work in the deformation bands than for uniform deformation. This leads to the main hypothesis that deformation banding occurs because it is energetically superior to uniform plastic deformation.

There are mathematical difficulties in formulating this intuitive concept of work minimization in the geometrically exact framework of finite elastoplastic deformation of single crystals. The approach proposed in Ortiz and Repetto (1999) and Ortiz et al. (2000) to describe sequential lamination towards single-slip domains, and further developments in Carstensen et al. (2002), Miehe et al. (2004), Conti and Theil (2005), Carstensen et al. (2008), Hansen et al. (2010), Kratochvíl et al. (2010), Kochmann and Hackl (2011), Homayonifar and Mosler (2011), Kumar et al. (2020), Yalçinkaya et al. (2012), Klusemann and Kochmann (2014), Anguige et al. (2018) and Dequiedt (2019), are based on the assumption of existence of an incremental potential. But in the multislip case, the slip-system interaction matrix is generally not symmetric (Peirce et al., 1982; Franciosi and Zaoui, 1991; Madec and Kubin, 2017), so that the incremental work or energy supplied does *not* act in general as an incremental potential (Petryk, 2003; Petryk and Kursa, 2013). If this constitutive matrix is preserved in its original, non-symmetric form then the open question was how to choose active slip systems from among the existing alternatives. The finite element method provides a powerful tool for the numerical study of deformation patterning, (e.g. Wang et al., 2018; Luan et al., 2020; Phalke et al., 2022), but it cannot replace the analytical approach like this presented here without rounding-off the yield-surface corners.

Recently, a new variational approach to the *non-potential* problems in rate-independent plasticity has been developed through the proposed 'quasi-extremal' energy principle (QEP) when ordinary stationarity or minimum principles fail (Petryk, 2020). The characteristic of this principle is that the minimized energy function or functional explicitly depends not only on variables undergoing variations but also on the unknown solution taken as a parameter. When solving the incremental problem of crystal plasticity, QEP reduces to the quasi-minimization of the incremental energy function in which the standard quadratic expression for deformation work is supplemented with a new bilinear form based on the skew part of the slip-system interaction matrix. The principle was applied by Petryk and Kursa (2022) to simulate uniform large plastic deformations of a single crystal, with automatic selection of currently active slip systems along the deformation path. This was done without any need to symmetrize the constitutive matrix of slip-system interaction.

The aim of this paper is to extend the latter work to a variational approach to deformation banding in the non-potential case.

We adopt the classical constitutive framework established by Hill and Rice (1972) for describing elastic–plastic finite deformation of metal single crystals, which has been widely used in various but essentially equivalent forms, cf. overviews by Asaro (1983), Havner (1992), Bassani (1994) and Roters et al. (2010). Selected examples of numerical simulation of deformation banding in fcc metal single crystals will be presented to show potentialities of the constitutive algorithm based on QEP. In the limit of a vanishingly small time step, the incremental solution tends to an exact solution to the constitutive rate-problem. The problem examined in this paper is local, i.e. formulated in the continuum mechanics framework at a single material point without slip-gradient effects. Extensions to non-local problems are possible since the quasi-extremal energy principle formulated in Petryk (2020) encompasses also the gradient-enhanced plasticity.

An overview of different algorithmic approaches to rate-independent crystal-plasticity was presented in de Souza Neto et al. (2008), and more recently in Petryk and Kursa (2022), so we do not repeat it here. The latter paper seems to be the first to explicitly show how to proceed in the rate-independent crystal plasticity if there are non-unique incremental solutions associated with *distinct* sets of active slip-systems in a *non-potential* case.

This paper has naturally its limitations. For the sake of simplicity, the generalized Schmid (normality) rule in the sense made precise by Hill and Rice (1972) is adopted. Non-associative plasticity (cf. Bigoni, 2012) is included in the recent variational energetic formulations for rate-independent thermodynamic systems (Petryk, 2020; Ulloa et al., 2021) along with aspects of gradient plasticity. Variational formulations and slip-system selection in the gradient-enhanced crystal plasticity are examined in other works, (e.g. Kuroda and Tvergaard, 2006, 2008; Svendsen and Bargmann, 2010; Reddy, 2013; Miehe et al., 2014; Erdle and Böhlke, 2017; Lewandowski and Stupkiewicz, 2018; Po et al., 2019; Dequiedt, 2021; Reddy et al., 2021), and are not addressed here. We do not circumvent the non-uniqueness problem in crystal plasticity by applying a rate-dependent (viscoplastic) model as it is frequently done, cf. Rice (1971), Peirce et al. (1983), Cuitiño and Ortiz (1993), Lebensohn and Tomé (1993), Anand and Kalidindi (1994), Raabe and Roters (2004), Dequiedt (2018), Prüger and Kiefer (2020), Zhang et al. (2021) and many other works. No dynamic effects due to interaction of multiple bands (Giarola et al., 2018) are considered here. The present work is limited to the rate-independent analysis of the quasi-static isothermal behaviour of ductile single crystals, with full account of geometric nonlinearity at large deformation.

The paper is organized as follows. The constitutive framework is recapitulated in Section 2 in the form suitable for the purposes of this work. In Section 3 the quasi-extremal energy principle (QEP) is specified for crystal plasticity, and its applicability to the selection of active slip systems is discussed. Section 4 contains the theoretical analysis of deformation banding in single crystals, which sheds light on the role of latent hardening in deformation pattern formation. Calculated examples of energetically preferable patterns of deformation bands are presented in Section 5 for Cu or Ni single crystals deformed plastically under macroscopic shear or channel-die compression. Section 6 contains a summary of the obtained theoretical and numerical results along with concluding remarks.

2. Constitutive framework

2.1. Rate-independent crystal plasticity

To take fully into account the dependence of the elastic–plastic response on the loading path, the constitutive description in a time-continuous setting is formulated in the rate form. The classical rate-independent constitutive framework for elastic–plastic crystals at finite isothermal deformation has been established by Hill and Rice (1972). It was reformulated later in an essentially equivalent form in Peirce et al. (1982), Asaro (1983), Bassani (1994) and has been widely used in the literature until now. It is presented below in a condensed form, limited to the aspects that are most essential for the purposes of the present work.

First, by using the known transformation rules (Hill, 1978; Petryk, 2000) and the standard notation,[1] the constitutive rate-equations of Hill

[1] Notation: Bold-face characters denote vectors or second-order tensors in a three-dimensional Euclidean space, and doublestruck capitals (like $\mathbb{C}$) denote fourth-order tensors. Direct juxtaposition of two tensors means simple contraction, a central dot – double contraction in the sense $\mathbf{A}\cdot\mathbf{B} = A_{ij}B_{ij}$, and $\otimes$ a tensor product. A superimposed mark -1, T or $-$T over a tensor symbol denotes an inverse, transpose or transposed inverse, respectively. A superimposed dot denotes the rate that is understood as the material time derivative in the one-sided (forward) sense, $\mathrm{d}/\mathrm{d}t^{+}$, and assumed to exist.

and Rice (1972) are reformulated in the Lagrangian description as follows

$$\dot{\mathbf{S}} = \mathbb{C}^{\mathrm{e}} \cdot \dot{\mathbf{F}} - \sum_{\beta\in\mathcal{N}} \boldsymbol{\Lambda}_{\mathrm{p}}^{\beta}\dot{\gamma}^{\beta}\,, \quad \dot{f}^{\alpha} = \boldsymbol{\Lambda}^{\alpha}\cdot\dot{\mathbf{F}} - \sum_{\beta\in\mathcal{N}} g^{\alpha\beta}\dot{\gamma}^{\beta}\,, \quad \alpha\in\mathcal{N}=\{1,\dots,N\}. \tag{1}$$

Throughout the paper, a Greek superscript (usually α or β, not an exponent) is used as an index of the crystallographic slip-system on which the rate of plastic shear (called slip rate) is denoted by $\dot{\gamma}^{\alpha}$, $\alpha = 1,\dots,N$ and associated with the corresponding yield function f^{α}. The respective N-dimensional vectors are denoted by $(\dot{\gamma}^{\alpha})$ and (f^{α}). If $\dot{\gamma}^{\beta}\equiv 0$, then the fourth-order elastic stiffness tensor $\mathbb{C}^{\mathrm{e}} = \overset{\mathrm{T}}{\mathbb{C}^{\mathrm{e}}}$ links the rate $\dot{\mathbf{S}}$ of the first Piola–Kirchhoff stress tensor $\mathbf{S}$ (called also Piola stress) to $\dot{\mathbf{F}}$, the rate of the deformation gradient $\mathbf{F}$ with respect to a fixed reference configuration that is chosen arbitrarily. Non-zero sum of $\boldsymbol{\Lambda}_{\mathrm{p}}^{\beta}\dot{\gamma}^{\beta}$ defines the direction of $\dot{\mathbf{S}}^{\mathrm{p}} = \dot{\mathbf{S}} - \mathbb{C}^{\mathrm{e}}\cdot\dot{\mathbf{F}}$ as the residual decrement of stress $\mathbf{S}$ after an infinitesimal cycle of $\mathbf{F}$, and $\boldsymbol{\Lambda}^{\alpha}$ is normal to the α-th yield-surface $f^{\alpha}=0$. The coefficients $\mathbb{C}^{\mathrm{e}}, \boldsymbol{\Lambda}_{\mathrm{p}}^{\alpha}, \boldsymbol{\Lambda}^{\alpha}, g^{\alpha\beta}$ of the *linear* rate-Eqs. (1) are known in the current state of the material denoted symbolically by $\mathcal{G}$, and depend on it in the manner specified in Section 2.2. Henceforth, we will restrict attention to $\boldsymbol{\Lambda}_{\mathrm{p}}^{\alpha} = \boldsymbol{\Lambda}^{\alpha}$, which implies the normality flow rule in the sense discussed by Hill and Rice (1972), see also (Asaro, 1983; Bigoni, 2012). The slip-system interaction matrix $(g^{\alpha\beta})$ will play an essential role in the later part of the paper. Further specifications will be provided in Section 2.2.

The principle of slip-system activity in the rate-independent framework reads

$$\dot{\gamma}^{\alpha}\ge 0, \quad f^{\alpha}\le 0, \quad f^{\alpha}\dot{\gamma}^{\alpha}=0 \qquad \forall\alpha\in\mathcal{N}. \tag{2}$$

It can be interpreted (Petryk, 2005) as the Kuhn–Tucker conditions for a minimum of the *virtual* work-rate density

$$\tilde{w}(\tilde{\gamma}^{\alpha},\dot{\mathbf{F}}) = \mathbf{S}\cdot\dot{\mathbf{F}} - \sum_{\alpha} f^{\alpha}\tilde{\gamma}^{\alpha}\,, \tag{3}$$

which is defined for arbitrary *virtual* slip rates $\tilde{\gamma}^{\alpha}$, not necessarily obeying the rule (2), while $\mathbf{S}$ and f^{α} are known in a given state $\mathcal{G}$. With the help of function $\tilde{w}$, the conditions (2) together take an *equivalent* form of the variational principle (Petryk and Kursa, 2013)

$$\dot{\gamma}^{\alpha} = \arg\min_{\tilde{\gamma}^{\alpha}\ge 0} \tilde{w}(\tilde{\gamma}^{\alpha},\dot{\mathbf{F}})\,. \tag{4}$$

The value of $\dot{\gamma}^{\alpha}$ is indeterminate for $f^{\alpha}=0$ from the principle (2) or (4) used in only one state $\mathcal{G}$. Unknown slip-rates $\dot{\gamma}^{\alpha}$ are to be determined (not necessarily uniquely) from the consistency conditions

$$\dot{f}^{\alpha}\le 0, \qquad \dot{f}^{\alpha}\dot{\gamma}^{\alpha}=0 \qquad \text{if } f^{\alpha}=0\,, \tag{5}$$

which makes the following constitutive rate-problem nonlinear (in fact, piecewise-linear).

Constitutive Rate-Problem:

In a given state $\mathcal{G}$ and for prescribed $\dot{\mathbf{F}}$, find $\dot{\gamma}^{\alpha}$ that satisfy the conditions $(1)_2$, (2) and (5) simultaneously $\forall\alpha\in\mathcal{N}$. (6)

2.2. Specification of constitutive equations

The relationships given in Section 2.1 are fundamental for the theoretical part of this paper. In this section, they are specified by typical assumptions of the conventional theory of crystal plasticity used in applications.

The common multiplicative split (Kröner, 1960) of a finite deformation gradient $\mathbf{F}$ is adopted,

$$\mathbf{F} = \mathbf{F}^{*}\mathbf{F}^{\mathrm{p}}\,, \quad \mathbf{F}^{*} = \mathbf{R}^{*}\mathbf{U}^{\mathrm{e}}\,, \qquad \det\mathbf{F}^{*}>0\,, \quad \det\mathbf{F}^{\mathrm{p}}=1\,, \tag{7}$$

where $\mathbf{F}^{\mathrm{p}}$ is the plastic deformation gradient, and $\mathbf{F}^{*}$ is the contraction of the lattice rotation tensor, $\mathbf{R}^{*}$, and the elastic stretch tensor relative to the stress-free configuration of the lattice, $\mathbf{U}^{\mathrm{e}}$.

Assume that elastic properties of the crystallographic lattice are unaffected by plastic flow and can be expressed by an elastic energy density function, $\phi^{e}(\mathbf{U}^{\mathrm{e}})$, whose exact form is inessential here. Then, at constant temperature,

$$\mathbf{S}^{*} = \frac{\partial\phi^{\mathrm{e}}}{\partial\mathbf{F}^{*}} = \mathbf{S}\overset{\mathrm{T}}{\mathbf{F}^{\mathrm{p}}}\,, \qquad \dot{\mathbf{S}}^{*} = \mathbb{C}^{*}\cdot\dot{\mathbf{F}}^{*}\,, \qquad \mathbb{C}^{*} = \frac{\partial^{2}\phi^{\mathrm{e}}}{\partial\mathbf{F}^{*}\partial\mathbf{F}^{*}}\,,$$
$$[\mathbb{C}^{*}]_{ijkl} = C^{*}_{ijkl} = F^{\mathrm{p}}_{jp}F^{\mathrm{p}}_{lq}C^{\mathrm{e}}_{ipkq}\,, \tag{8}$$

by using Eqs. (7) and the standard chain rule of differentiation, where the last equation is written down in Cartesian components with the summation convention for repeated indices.

A yield function f^{α} is defined as the difference between the generalized shear stress τ^{α} resolved on the α-th slip system, such that $\sum_{\alpha}\tau^{\alpha}\dot{\gamma}^{\alpha}$ is the plastic work-rate per unit reference volume, and its critical (threshold) value, viz.

$$f^{\alpha} = \tau^{\alpha} - \tau^{\alpha}_{\mathrm{cr}}\,, \qquad \tau^{\alpha} = \boldsymbol{\Pi}\cdot\mathbf{N}^{\alpha}\,, \qquad \boldsymbol{\Pi} = \overset{\mathrm{T}}{\mathbf{F}^{*}}\mathbf{S}^{*}\,, \tag{9}$$

where $\boldsymbol{\Pi}$ denotes the Mandel stress (Mandel, 1971). The critical resolved shear stresses, $\tau^{\alpha}_{\mathrm{cr}}$, obey the conventional incremental hardening law

$$\dot{\tau}^{\alpha}_{\mathrm{cr}} = \sum_{\beta} h^{\alpha\beta}\,\dot{\gamma}^{\beta}\,, \tag{10}$$

where the hardening moduli $h^{\alpha\beta}$ may depend on the history of plastic slips. Opposite slips on a given slip plane are treated as different slip systems (because each $\dot{\gamma}^{\alpha}\ge 0$), so that the respective values of $\tau^{\alpha}_{\mathrm{cr}}$ are positive but need not be equal. This admits a back-stress related to the split of $\tau^{\alpha}_{\mathrm{cr}}$ into energetic and dissipative parts. The split may be arbitrary here, cf. Petryk and Kursa (2015, Remark 2), therefore the related thermodynamic description is omitted in this paper.

Evolution of the plastic deformation gradient $\mathbf{F}^{\mathrm{p}}$, caused by the activity of multiple slip-systems, is governed by (Rice, 1971)

$$\dot{\mathbf{F}}^{\mathrm{p}}(\mathbf{F}^{\mathrm{p}})^{-1} = \sum_{\alpha}\mathbf{N}^{\alpha}\dot{\gamma}^{\alpha}\,, \qquad \mathbf{N}^{\alpha} = \mathbf{m}^{\alpha}\otimes\mathbf{n}^{\alpha}\,, \qquad \mathbf{m}^{\alpha}\cdot\mathbf{n}^{\alpha}=0\,, \tag{11}$$

where $(\mathbf{m}^{\alpha},\mathbf{n}^{\alpha})$ define slip direction and slip-plane normal, respectively, of the α-th slip system in the stress-free (intermediate) configuration of the crystallographic lattice. By Jacobi's formula for the rate of $\det\mathbf{F}^{\mathrm{p}}$, the assumption $\mathbf{m}^{\alpha}\cdot\mathbf{n}^{\alpha}=0$ implies that the plastic deformation is isochoric, $\det\mathbf{F}^{\mathrm{p}}\equiv 1$.

To complete specification of the quantities involved in the constitutive framework given in Section 2.1, it remains to define state-dependent coefficients $\boldsymbol{\Lambda}^{\alpha}$ and $g^{\alpha\beta}$ of the constitutive rate-Eqs. (1), assuming the normality rule with $\boldsymbol{\Lambda}^{\alpha}_{\mathrm{p}} = \boldsymbol{\Lambda}^{\alpha}$. In full agreement with Hill and Rice (1972), it has been shown that the definition (9) and geometric nonlinearity relationships imply that (Petryk and Kursa, 2013)

$$\boldsymbol{\Lambda}^{\alpha} = \left(\mathbb{C}^{*}\cdot\mathbf{F}^{*}\mathbf{N}^{\alpha} + \mathbf{S}^{*}\overset{\mathrm{T}}{\mathbf{N}^{\alpha}}\right)\overset{-\mathrm{T}}{\mathbf{F}^{\mathrm{p}}}\,, \tag{12}$$

$$g^{\alpha\beta} = h^{\alpha\beta} + g^{\alpha\beta}_{\mathrm{geom}}\,, \qquad g^{\alpha\beta}_{\mathrm{geom}} = \mathbf{F}^{*}\mathbf{N}^{\alpha}\cdot\mathbb{C}^{*}\cdot\mathbf{F}^{*}\mathbf{N}^{\beta} + \boldsymbol{\Pi}\cdot\mathbf{N}^{\beta}\mathbf{N}^{\alpha}\,. \tag{13}$$

It follows that matrix $(g^{\alpha\beta})$ is generally non-symmetric for two independent reasons: $(h^{\alpha\beta})\neq(h^{\beta\alpha})$ or $\boldsymbol{\Pi}\cdot(\mathbf{N}^{\beta}\mathbf{N}^{\alpha}-\mathbf{N}^{\alpha}\mathbf{N}^{\beta})\neq 0$. Unlike in the reference (*op. cit*), the approach in this paper does not require any symmetrization of $(g^{\alpha\beta})$; see also (Peirce et al., 1982).

The above constitutive description of the conventional crystal plasticity at finite deformation, or its equivalent, is the basis for determining the computational model for a given metal crystal.

2.3. Finite time increments

For computational purposes, Constitutive Rate-Problem (6) is reformulated in terms of increments over a small but finite time interval $[t_n, t_{n+1}]$. The end-point values of a quantity ψ evaluated at t_n and t_{n+1}

are denoted by ψ_n and ψ_{n+1}, respectively, and the increment by a prefix Δ, $\Delta\psi := \psi_{n+1} - \psi_n$ corresponding to $\Delta t := t_{n+1} - t_n$.

An implicit backward-Euler difference scheme is applied to solve approximately the incremental problem that results from constitutive assumptions given in Section 2.1. For consistency with the constitutive rate Eqs. (1) it is required that upon substituting

$$\dot\gamma^\alpha = \frac{\Delta\gamma^\alpha}{\Delta t}, \qquad \dot{\mathbf{F}} = \frac{\Delta\mathbf{F}}{\Delta t}, \tag{14}$$

the following conditions hold true

$$\mathbf{S}_{n+1} - \mathbf{S}_n = \hat\Delta\mathbf{S} + o(\Delta t), \qquad f^\alpha_{n+1} - f^\alpha_n = \hat\Delta f^\alpha + o(\Delta t), \quad \alpha \in \mathcal{N}, \tag{15}$$

with $o(\Delta t)/\Delta t \to 0$ as $\Delta t \to 0$. The *approximate* increments, $\hat\Delta\mathbf{S}, \hat\Delta f^\alpha$, are obtained by *backward* time integration of Eqs. (1) starting from t_{n+1} and keeping the coefficients fixed,

$$\hat\Delta\mathbf{S} = \mathbb{C}^{\mathrm{e}}_{n+1}\cdot\Delta\mathbf{F} - \sum_{\alpha\in\mathcal{N}} \boldsymbol{\Lambda}^\alpha_{n+1}\Delta\gamma^\alpha, \qquad \hat\Delta f^\alpha = \boldsymbol{\Lambda}^\alpha_{n+1}\cdot\Delta\mathbf{F} - \sum_{\beta\in\mathcal{N}} g^{\alpha\beta}_{n+1}\Delta\gamma^\beta. \tag{16}$$

To satisfy Eqs. (1), the coefficients $\mathbb{C}^{\mathrm{e}}_t$, $\boldsymbol{\Lambda}^\alpha_t$ and $g^{\alpha\beta}_t$ are assumed be uniformly continuous with respect to time t. $\Delta\gamma^\alpha$ is identified with an unknown increment of shear on the α-th slip-system, and $\Delta\mathbf{F}$ with an increment of the deformation gradient whose components may be partially known.

The two sets of conditions (2) and (5) for plastic slip-system activity are reduced to so-called discrete consistency conditions,

$$\Delta\gamma^\alpha \ge 0 \quad \text{and} \quad f^\alpha_{n+1} \le 0 \quad \text{and} \quad f^\alpha_{n+1}\,\Delta\gamma^\alpha = 0 \qquad \forall\alpha\in\mathcal{N}, \tag{17}$$

assuming that $f^\alpha_n \le 0$ from the previous time step.

A time-discrete counterpart to Constitutive Rate-Problem (6) in Section 2.1 takes the following form.

Incremental Constitutive Problem:

Given the state $\mathcal{G}_n$ *with* $f^\alpha_n \le 0$, $\Delta\mathbf{F}$ *and relationship* $(15)_2$,

find $\Delta\gamma^\alpha$ *that satisfy the conditions* (17) $\forall\alpha\in\mathcal{N}$. (18)

As noted by Petryk and Kursa (2022), a solution to Incremental Constitutive Problem (18) provides in the limit as $\Delta t \to 0$ an *exact* solution to the Constitutive Rate-Problem (6) formulated at t_n. For a finite time step, the following expression for f^α_{n+1} will be used in calculations,

$$f^\alpha_{n+1} := \tau^\alpha_{n+1} - \tau^\alpha_{\mathrm{cr}\,n+1}, \tag{19}$$

where τ^α_{n+1} is defined, as in Eq. (9), by the projection of the Mandel stress $\boldsymbol{\Pi}_{n+1}$ on $\mathbf{N}^\alpha$, and $\tau^\alpha_{\mathrm{cr}\,n+1}$ is calculated incrementally using the hardening law (10).

3. Quasi-extremal energy principle

The reader is referred to Petryk (2020) for a detailed exposition of the concept of a quasi-extremal energy principle in a general case. It specification developed in Petryk and Kursa (2022) for crystal plasticity is briefly outlined below. The formulation in the rates is omitted, and we go directly to considerations for a finite time step.

3.1. Incremental constitutive quasi-potential

The key step is to construct an incremental energy function as a strong variation of the work density functional at the end of a time step. This incremental energy function differs from the usual incremental work density Δw only by the last term,

$$\Delta\varepsilon(\tilde\gamma^\alpha, \Delta\mathbf{F}; \Delta\gamma^\alpha) = \Delta w(\tilde\gamma^\alpha, \Delta\mathbf{F}) + \frac{1}{2}\sum_{\alpha,\beta\in\mathcal{N}} \tilde\gamma^\alpha(g^{\alpha\beta}_{n+1} - g^{\beta\alpha}_{n+1})\Delta\gamma^\beta, \tag{20}$$

where Δw corresponds to a *straight* path along which *virtual* increments of slips $\gamma^\alpha(t)$ vary in a time step $t \in [t_n, t_{n+1}]$ proportionally from 0 to $\tilde\gamma^\alpha$ for all α. Δw is affected only by the symmetric part of matrix $(g^{\alpha\beta}_{n+1})$, while a skew part of $(g^{\alpha\beta}_{n+1})$ and parameters $\Delta\gamma^\alpha$ affect only the last term in Eq. (20). It follows that

$$\Delta\varepsilon(\Delta\gamma^\alpha, \Delta\mathbf{F}; \Delta\gamma^\alpha) = \Delta w(\Delta\gamma^\alpha, \Delta\mathbf{F}), \tag{21}$$

since the last term present in Eq. (20) then vanishes as a quadratic form with a skew matrix. However, the last term in Eq. (20) is crucial for a correct extension of the incremental work minimization to non-symmetric matrices $(g^{\alpha\beta})$ when Δw does not act as a constitutive potential for variable $\Delta\gamma^\alpha$.

When evaluated to second-order with respect to $\Delta t = t_{n+1} - t_n$ by *backward* time integration, Δw reads (Petryk and Kursa, 2022)

$$\Delta w(\tilde\gamma^\alpha, \Delta\mathbf{F}) = \mathbf{S}_{n+1}\cdot\Delta\mathbf{F} - \sum_{\alpha\in\mathcal{N}} f^\alpha_{n+1}\tilde\gamma^\alpha - \Delta_2 w(\tilde\gamma^\alpha, \Delta\mathbf{F}), \tag{22}$$

where $\Delta_2 w$ is the second-order work expression

$$\Delta_2 w(\tilde\gamma^\alpha, \Delta\mathbf{F}) = \frac{1}{2}\Delta\mathbf{F}\cdot\mathbb{C}^{\mathrm{e}}_{n+1}\cdot\Delta\mathbf{F} - \sum_{\alpha\in\mathcal{N}}\left(\boldsymbol{\Lambda}^\alpha_{n+1}\cdot\Delta\mathbf{F}\right)\tilde\gamma^\alpha + \frac{1}{2}\sum_{\alpha,\beta\in\mathcal{N}}\tilde\gamma^\alpha g^{\alpha\beta}_{n+1}\tilde\gamma^\beta. \tag{23}$$

Note that the energy function $\Delta\varepsilon$ is defined with the coefficients evaluated at t_{n+1} for a yet unknown incremental solution $\Delta\gamma^\alpha$ as a parameter. If $\tilde\gamma^\alpha$ coincides with a solution $\Delta\gamma^\alpha$ then the incremental work expression simplifies, on account of Eqs. $(17)_3$ and (16), to

$$\Delta w(\Delta\gamma^\alpha, \Delta\mathbf{F}) = \mathbf{S}_{n+1}\cdot\Delta\mathbf{F} - \Delta_2 w(\Delta\gamma^\alpha, \Delta\mathbf{F}) \tag{24}$$

with

$$\Delta_2 w(\Delta\gamma^\alpha, \Delta\mathbf{F}) = \frac{1}{2}\hat\Delta\mathbf{S}\cdot\Delta\mathbf{F} \tag{25}$$

since the remaining term $\sum_\alpha \hat\Delta f^\alpha\Delta\gamma^\alpha = o((\Delta t)^2)$ (cf. the consistency condition $(5)_2$) can be omitted in this second-order work expression.

The Taylor decomposition of $\Delta\varepsilon$ takes the form

$$\begin{aligned}\Delta\varepsilon(\tilde\gamma^\alpha, \Delta\mathbf{F}; \Delta\gamma^\alpha) = {}& \Delta\varepsilon(\Delta\gamma^\alpha, \Delta\mathbf{F}; \Delta\gamma^\alpha) + \Delta_1\varepsilon(\tilde\gamma^\alpha, \Delta\gamma^\alpha) + \Delta_2\varepsilon(\tilde\gamma^\alpha, \Delta\gamma^\alpha)\\ &+ o(\tilde\gamma^\alpha - \Delta\gamma^\alpha)^2,\end{aligned} \tag{26}$$

where

$$\begin{aligned}\Delta\varepsilon(\Delta\gamma^\alpha, \Delta\mathbf{F}, \Delta\gamma^\alpha) = {}& \Delta w(\Delta\gamma^\alpha, \Delta\mathbf{F}),\\ \Delta_1\varepsilon(\tilde\gamma^\alpha, \Delta\gamma^\alpha) = {}& -\sum_{\alpha\in\mathcal{N}} f^\alpha_{n+1}(\tilde\gamma^\alpha - \Delta\gamma^\alpha),\\ \Delta_2\varepsilon(\tilde\gamma^\alpha, \Delta\gamma^\alpha) = {}& \frac{1}{2}\sum_{\alpha,\beta\in\mathcal{N}}(\tilde\gamma^\alpha - \Delta\gamma^\alpha)g^{\alpha\beta}_{n+1}(\tilde\gamma^\beta - \Delta\gamma^\beta).\end{aligned} \tag{27}$$

The key result is (Petryk and Kursa, 2022)

$$\mathbf{S}_{n+1} = \frac{\partial\Delta\varepsilon}{\partial\Delta\mathbf{F}}, \qquad f^\alpha_{n+1} = -\left.\frac{\partial\Delta\varepsilon}{\partial\tilde\gamma^\alpha}\right|_{\tilde\gamma^\beta=\Delta\gamma^\beta}, \tag{28}$$

so that function $\Delta\varepsilon$ acts precisely as a constitutive potential for $\mathbf{S}_{n+1}$ and a *quasi-potential* for f^α_{n+1}.

3.2. Quasi-extremal energy principle (QEP) for incremental slips

In close analogy to Petryk (2020, Theorem 2) but with the modification resulting from finite increments, the following proposition holds true at a material point.

Proposition 1 (*Quasi-extremal energy principle for incremental slips*)**.** *A solution* $(\Delta\gamma^\alpha)$ *to the following quasi-extremal energy principle (QEP):*

$$(\Delta\gamma^\alpha) = \arg\min_{\tilde\gamma^\alpha\ge 0}\Delta\varepsilon(\tilde\gamma^\alpha, \Delta\mathbf{F}; \Delta\gamma^\alpha) \tag{29}$$

(i) solves Incremental Constitutive Problem (18)*, and*
(ii) satisfies additionally the condition

$$\sum_{\alpha,\beta\in\mathcal{N}}(\tilde\gamma^\alpha - \Delta\gamma^\alpha)g^{\alpha\beta}_{n+1}(\tilde\gamma^\beta - \Delta\gamma^\beta) \ge 0 \qquad \forall\tilde\gamma^\alpha \ge 0 \quad \textit{subject to} \quad f^\alpha_{n+1}\tilde\gamma^\alpha = 0. \tag{30}$$

Proof. It coincides with the proof of Proposition 3 in Petryk and Kursa (2022).

The left-hand expression of inequality (30) represents the second variation of the incremental energy function $\Delta\varepsilon$ in a direction of $\delta\gamma^\alpha = (\tilde{\gamma}^\alpha - \Delta\gamma^\alpha)$, cf. Eq. (26). Therefore, condition (30) can be interpreted as the energy condition for stability of the plastic deformation path corresponding to a solution $\Delta\gamma^\alpha$ to Incremental Constitutive Problem (18).

From Eq. $(16)_2$ it can be seen that $\sum_\beta g^{\alpha\beta}_{n+1}\delta\gamma^\beta = -\delta f^\alpha_{n+1}$, a variation of f^α_{n+1} for fixed $\Delta\mathbf{F}$, with a negative sign. Inequality (30) thus means that the scalar product of a perturbation $(\delta\gamma^\alpha)$ of incremental slips and the associated perturbation (δf^α) of yield functions is non-positive for given $\Delta\mathbf{F}$. This can be interpreted as a contractivity property that supports the treatment of inequality (30) as the path stability condition.

For the potential problem when the skew part of matrix $(g^{\alpha\beta})$ vanishes, QEP (29) reduces to straightforward minimization of Δw referred to as the incremental energy minimization (Petryk, 2003), initiated in Petryk (1982).

Proposition 1 has provided a theoretical basis for the constitutive algorithm which is described in detail in Petryk and Kursa (2022). A modified algorithmic expression for the incremental deformation work Δw is used there to improve convergence of the iterations required to solve QEP (29). Lagrange multipliers are treated as additional variables to satisfy the unilateral constraints imposed on $\tilde{\gamma}^\alpha$. The non-smooth and constrained non-convex minimization sub-problem in QEP (29) is reduced to a smooth and unconstrained optimization problem by using the augmented Lagrangian method (Bertsekas, 1996). The solution to the k-th sub-problem is iteratively used as input to the $(k+1)$-th sub-problem until QEP (29) is satisfied within the given tolerance. Specifically, the iterations are repeated until the conditions (17) are met with the required accuracy. The algorithm was implemented in the scientific computing environment *Mathematica* (www.wolfram.com) using the built-in function *FindMinimum* for an unconstrained search for the minimum of a non-convex function, here the augmented Lagrangian based on the incremental energy function $\Delta\varepsilon$.

3.3. Selection of active slip-systems by QEP

In general, Incremental Constitutive Problem (18) can have non-unique solutions which correspond to different sets of active slip systems. In such cases, the quasi-extremal energy principle QEP (29) through the resulting additional condition (30) provides a criterion of selection of the active slip-system set (Petryk, 2020). It is based on the energy criterion of path stability and can thus be given a physical meaning, being not based on arbitrarily assumed imperfections or random selection. This is a generalization of the incremental energy minimization approach limited to problems of potential type that exhibit the needed symmetry property (Petryk, 2003), to non-potential problems of crystal plasticity with a non-symmetric slip-system interaction matrix, $(g^{\alpha\beta}) \neq (g^{\beta\alpha})$. The 'ambiguity' in selecting the set of active slip systems is frequently traced back to Taylor (1938b), although the consistency conditions were not considered at that time. The QEP-based approach overcomes this long-standing difficulty in the rate-independent crystal plasticity without the need to symmetrize the matrix $(g^{\alpha\beta})$.

The QEP-based crystal plasticity algorithm developed in Petryk and Kursa (2022) enables automatic change of the set of active slip systems along the calculated path of plastic deformation whenever the minimum required in Eq. (29) is no longer met for the previous set. Typically, such a change accompanies switching between different corners or edges on the current yield surface for the crystal. The mechanism of automatic selection of a new set of active slip systems by incremental energy minimization was examined in Petryk and Kursa (2015) in the case of the selectively symmetrized matrix $(g^{\alpha\beta})$. It remains essentially unchanged when QEP is applied to a non-symmetric matrix $(g^{\alpha\beta})$, as demonstrated in Petryk and Kursa (2022) and also by numerical examples presented in Section 5 of this paper. The set $\mathcal{A}$ of currently active slip systems is determined as part of the solution to the minimization sub-problem in QEP (29), in distinction to other approaches where $\mathcal{A}$ is *assumed* before solving the system of equations $f^{\alpha\in\mathcal{A}} = 0$.

4. Energy approach to deformation banding

4.1. Energetically preferable pattern formation

The formation of a non-uniform deformation pattern under conditions that would correspond to homogeneous deformation can be considered as a symptom of instability in the energy sense of a uniform quasi-static deformation *path*, which in plastic solids is usually *not* accompanied by the loss of stability of equilibrium (Petryk, 1982). Conditions for *material stability* can be derived by restricting the virtual deviation from the examined deformation process (path) to a neighbourhood of an interior material point.

The corresponding integral condition for a minimum of a functional, expressed in terms of its properties at a point by Morrey (1952), was applied to elastic strain energy by Ball (1977) and extended to the incremental deformation work that includes plastic dissipation by Petryk (1992). This has been done under the assumption that incremental work density Δw can be expressed as a function of the incremental deformation gradient $\Delta\mathbf{F}$. By negation of a minimum, the following condition for *instability* of a uniform deformation mode $\Delta\mathbf{F}_0$ has been obtained,

$$\frac{1}{|\mathcal{M}|}\int_{\mathcal{M}} \Delta w(\Delta\mathbf{F}_0 + \nabla\mathbf{w}(\mathbf{X}))\,\mathrm{d}\mathbf{X} < \Delta w(\Delta\mathbf{F}_0) \quad \text{for some } \underline{\mathbf{w}} : \mathbf{w} = \mathbf{0} \text{ over } \partial\mathcal{M}\,, \tag{31}$$

where $\mathcal{M}$ of volume $|\mathcal{M}|$ is a bounded domain in the reference configuration, which without loss of generality can be chosen arbitrarily, and $\underline{\mathbf{w}}$ can be any continuous and piecewise differentiable perturbation field on $\mathcal{M}\cup\partial\mathcal{M}$. Inequality (31) means that mechanical work can be extracted from the *deforming* material element $\mathcal{M}$ embedded in a continuum being unperturbed elsewhere.

In the problem considered in this paper, Δw depends not only on $\Delta\mathbf{F}$ but also on slip increments $\Delta\gamma^\alpha$ which are determined from the quasi-extremal energy principle, QEP (29). Accordingly, the condition (31) for material instability is now extended to

$$\frac{1}{|\mathcal{M}|}\int_{\mathcal{M}} \Delta w(\Delta\gamma^\alpha(\mathbf{X}), \Delta\mathbf{F}_0 + \nabla\mathbf{w}(\mathbf{X}))\,\mathrm{d}\mathbf{X} < \Delta w(\Delta\gamma^\alpha_0, \Delta\mathbf{F}_0)$$
$$\text{for some } \underline{\mathbf{w}} : \ \mathbf{w} = \mathbf{0} \text{ over } \partial\mathcal{M}\,, \tag{32}$$

where

$$(\Delta\gamma^\alpha)(\mathbf{X}) = \arg\min_{\tilde{\gamma}^\alpha\geq 0} \Delta\varepsilon(\tilde{\gamma}^\alpha, \Delta\mathbf{F}_0 + \nabla\mathbf{w}(\mathbf{X}); \Delta\gamma^\alpha(\mathbf{X}))\,. \tag{33}$$

The unknown field $\underline{\mathbf{w}}$ represents the incremental deformation pattern searched.

The incremental work minimization approach based on the condition (32) was applied in Petryk and Kursa (2013) to deformation banding in the case when the incremental work density Δw played the role of a constitutive potential. Under a similar assumption, the related approach was developed earlier by M. Ortiz and co-workers, see the references given in the Introduction. Here, the previous work is extended to the case (33) when the energy function $\Delta\varepsilon$, rather than the incremental work density Δw itself, is used as the constitutive *quasi-potential* for determining incremental slips along with the unknown set of active slip systems at a material point. As discussed above, this generalization has its physical motivation in the lack of symmetry of the slip-system interaction matrix $(g^{\alpha\beta})$.

4.2. Deformation bands

Consider a pattern of two families of parallel deformation bands of a unit reference normal $\mathbf{n}$, such that a pair $(\Delta\gamma^\alpha(\mathbf{X}), \nabla\mathbf{w}(\mathbf{X}))$ alternates between two values, $(\Delta\gamma_1^\alpha, \nabla\mathbf{w}_1)$ and $(\Delta\gamma_2^\alpha, \nabla\mathbf{w}_2)$, corresponding to two different sets $\mathcal{A}_1, \mathcal{A}_2$ of active slip systems (Fig. 1). The incremental statical and kinematical compatibility conditions across the band interfaces read

$$(\Delta\mathbf{S}_1 - \Delta\mathbf{S}_2)\mathbf{n} = \mathbf{0} \qquad \text{and} \qquad \Delta\mathbf{F}_1 - \Delta\mathbf{F}_2 = \Delta\mathbf{b}\otimes\mathbf{n} \tag{34}$$

for some non-zero vector $\Delta\mathbf{b}$ and some $|\mathbf{n}| = 1$. In terms of the overall deformation gradient increment, $\Delta\mathbf{F}_0 = \eta\Delta\mathbf{F}_1 + (1-\eta)\Delta\mathbf{F}_2$, the deformation gradient increments in the bands are

$$\Delta\mathbf{F}_1 = \Delta\mathbf{F}_0 + (1-\eta)\Delta\mathbf{b}\otimes\mathbf{n}\,, \qquad \Delta\mathbf{F}_2 = \Delta\mathbf{F}_0 - \eta\Delta\mathbf{b}\otimes\mathbf{n}\,, \qquad 0\le\eta\le 1. \tag{35}$$

Suppose that the bands are long and of relatively small spacing H, and that the banded domain is surrounded by a boundary layer within which $\mathbf{w}$ tends to zero as $\partial\mathcal{M}$ is approached. A rigorous construction known in the context of finite elasticity (Chipot and Kinderlehrer, 1988) leads to a field $\underline{\mathbf{w}}$ of uniformly bounded gradient $\nabla\mathbf{w}$, such that

$$\frac{1}{|M|}\int_{\mathcal{M}} \Delta w(\Delta\gamma^\alpha(\mathbf{X}), \Delta\mathbf{F}_0 + \nabla\mathbf{w}(\mathbf{X}))\,\mathrm{d}\mathbf{X}$$
$$= \eta\Delta w(\Delta\gamma_1^\alpha, \Delta\mathbf{F}_1) + (1-\eta)\Delta w(\Delta\gamma_2^\alpha, \Delta\mathbf{F}_2) + O(H)\,, \tag{36}$$

where $O(H)\to 0$ as $H\to 0$. Consequently, the energy condition (32) for material instability is satisfied for band spacing H sufficiently small (so that $O(H)$ is less than the difference in inequality (32) after substituting expression (36)) if

$$\Delta\bar{w} = \eta\Delta w(\Delta\gamma_1^\alpha, \Delta\mathbf{F}_1) + (1-\eta)\Delta w(\Delta\gamma_2^\alpha, \Delta\mathbf{F}_2) < \Delta w(\Delta\gamma_0^\alpha, \Delta\mathbf{F}_0)$$
$$\text{subject to Eqs. (33) and (35) for some } \Delta\mathbf{b}, \mathbf{n}, \eta\,. \tag{37}$$

It is possible to extend condition (37) to size-effects by adding to $\Delta\bar{w}$ the energy contribution of the band interfaces and of the boundary layer at $\partial\mathcal{M}$, in analogy to Chin and Wonsiewicz (1969), Ortiz and Repetto (1999) and Ortiz et al. (2000). However, as mentioned in the Introduction, the size-independent consequences of QEP are isolated for study here, so a size-dependent analysis is beyond the scope of this article. Accordingly, the attention is limited to volume fractions of the bands, not their width. The deformation pattern is determined by the free variables in the energy criterion (38) subject to (35) and (39), that is, by the volume fraction and orientation of the bands together with the incremental deformation gradient and the incremental slips within the bands, while the width and placement of individual bands are undefined.

As in Eq. (33), unknown $\Delta\gamma^\alpha$ are determined from QEP (29). Accordingly, the incremental work criterion for the onset of deformation banding takes the form

$$\min_{\Delta\mathbf{b},\mathbf{n},\eta} \big(\eta\Delta w_1 + (1-\eta)\Delta w_2\big) < \Delta w_0 \qquad \text{subject to Eqs. (35) and (39),} \tag{38}$$

where

$$\Delta w_i = \Delta w(\Delta\gamma_i^\alpha, \Delta\mathbf{F}_i)\,, \qquad (\Delta\gamma_i^\alpha) = \arg\min_{\tilde{\gamma}^\alpha\ge 0} \Delta\epsilon(\tilde{\gamma}^\alpha, \Delta\mathbf{F}_i; \Delta\gamma_i^\alpha)\,, \qquad i = 0,1,2\,. \tag{39}$$

A novelty in the present approach is the use of the quasi-extremal energy principle QEP (29) in Eqs. (33) and (39) for determining the sets of active slip systems and increments $\Delta\gamma^\alpha$.

Finding the minimum in criterion (38) is a complex task that generally requires an appropriate numerical approach. There may be more than one local minimum of the left-hand expression, and the lowest value is not necessarily the most physically significant; examples will be presented in Section 5.

To facilitate the minimization task and investigate in advance the circumstances under which inequality (38) can have solutions, in the next subsection we will address the incipient deformation banding treated as a bifurcation problem in a given homogeneous state.

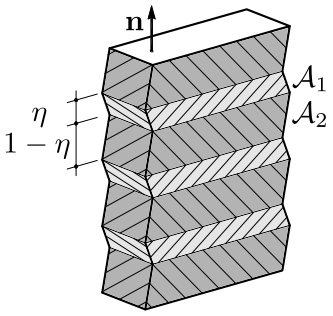

Fig. 1. Two families of deformation bands with different sets $\mathcal{A}_1, \mathcal{A}_2$ of active slip-systems.

4.3. Incipient deformation banding

The current homogeneous state of the material is regarded as known. Consider an incipient deformation banding mode illustrated in Fig. 1, expressed now in the rate form, which satisfies the statical and kinematical compatibility conditions across discontinuity surfaces, viz.

$$(\dot{\mathbf{S}}_1 - \dot{\mathbf{S}}_2)\mathbf{n} = \mathbf{0} \qquad \text{and} \qquad \dot{\mathbf{F}}_1 - \dot{\mathbf{F}}_2 = \dot{\mathbf{b}}\otimes\mathbf{n}\,. \tag{40}$$

Rice's familiar condition for existence of a non-trivial solution to Eqs. (40) with a non-zero jump has the form $\det\mathbf{Q}_\mathrm{n} = 0$, where $\mathbf{Q}_\mathrm{n}$ is the acoustic tensor based on the tangent stiffness moduli which are assumed the same within and outside a localization band (Rice, 1977). That approach is not applicable here since the sets of active slip-systems in the bands, $\mathcal{A}_1$ and $\mathcal{A}_2$, are different and not known a priori, so the tangent stiffness moduli in the bands are different and unknown.

A more general approach has been developed by Petryk (2000), which does not require knowledge of the set of actually active inelastic deformation mechanisms. Namely, the *purely elastic* acoustic tensor $\mathbf{Q}_\mathrm{n}^\mathrm{e}$ has been used that is defined by $(\mathbf{Q}_\mathrm{n}^\mathrm{e})_{ik} = (\mathbb{C}^\mathrm{e})_{ipkq}n_p n_q$, in Cartesian components with the summation convention. Given that $\mathbf{Q}_\mathrm{n}^\mathrm{e}$ is non-singular, $\det\mathbf{Q}_\mathrm{n}^\mathrm{e} \neq 0$ which is the ellipticity condition for the *purely elastic* response, the following matrix has been defined,

$$g_\mathrm{band}^{\alpha\beta} = g^{\alpha\beta} - (\boldsymbol{\Lambda}^\alpha\mathbf{n})\cdot\overset{-1}{\mathbf{Q}_\mathrm{n}^\mathrm{e}}(\boldsymbol{\Lambda}^\beta\mathbf{n}), \qquad g_\mathrm{band}^{\mathcal{A}} = (g_\mathrm{band}^{\alpha\beta}) \text{ with } \alpha,\beta\in\mathcal{A}\,, \tag{41}$$

where the slip-system set $\mathcal{A}$ is arbitrary. This matrix is known in a given state for a given band orientation $\mathbf{n}\neq\mathbf{0}$, which is not marked in the matrix symbol to simplify the notation.

The exclusion condition for incipient deformation banding from a given homogeneous state, established in Petryk (2000), states that the problem (40) for given $\mathbf{n}\neq\mathbf{0}$ admits only the trivial solution ($\dot{\mathbf{b}} = \mathbf{0}$) if all principal minors of the matrix $(g_\mathrm{band}^{\mathcal{P}})$ defined by Eq. (41) for the set $\mathcal{P} = \{\alpha\in\mathcal{N} \;:\; f^\alpha = 0\}$ of the potentially active systems are positive, viz.

$$\det g_\mathrm{band}^{\mathcal{A}} > 0 \qquad \forall\mathcal{A}\subseteq\mathcal{P}\,. \tag{42}$$

In the terminology of Cottle et al. (1992), it means that matrix $g_\mathrm{band}^{\mathcal{P}}$ is a **P**-matrix. It is pointed out that fulfilment of condition (42) excludes incipient deformation banding for any possible unloading at the bifurcation instant within the bands of reference orientation $\mathbf{n}$.

The fundamental role played by matrix g_band can be highlighted as follows. Suppose that a fully admissible banding mode $(\dot{\mathbf{b}}, \mathbf{n})$ exists which satisfies Eqs. (40) for slip rates $\dot{\gamma}_1^\alpha \ge 0, \dot{\gamma}_2^\alpha \ge 0$ in the bands (1) and (2), respectively. The joint set of active slip systems is denoted by

$$\mathcal{B} = \{\alpha\in\mathcal{P} \;:\; \dot{\gamma}_1^\alpha > 0 \text{ or } \dot{\gamma}_2^\alpha > 0\} = \mathcal{A}_1\cup\mathcal{A}_2\,. \tag{43}$$

On writing down the constitutive rate Eq. $(1)_2$ for each band and subtracting them, on account of Eq. $(40)_2$ we obtain

$$f_1^\alpha - f_2^\alpha = \dot{\mathbf{b}}\cdot\boldsymbol{\Lambda}^\alpha\mathbf{n} - \sum_{\beta\in\mathcal{B}} g^{\alpha\beta}(\dot{\gamma}_1^\beta - \dot{\gamma}_2^\beta)\,, \qquad \alpha\in\mathcal{B}. \tag{44}$$

In turn, a similar action but applied to the constitutive rate Eq. $(1)_1$ gives

$$(\dot{\mathbf{S}}_1 - \dot{\mathbf{S}}_2)\mathbf{n} = \mathbf{Q}_{\mathrm{n}}^{\mathrm{e}}\dot{\mathbf{b}} - \sum_{\alpha\in B}(\dot\gamma_1^\alpha - \dot\gamma_2^\alpha)\boldsymbol{\Lambda}^\alpha\mathbf{n}\,. \tag{45}$$

The value of this expression must be $\mathbf{0}$ on account of Eq. $(40)_1$, so that (Petryk, 2000)

$$\dot{\mathbf{b}} = \overset{-1}{\mathbf{Q}_{\mathrm{n}}^{\mathrm{e}}}\sum_{\alpha\in B}(\dot\gamma_1^\alpha - \dot\gamma_2^\alpha)\boldsymbol{\Lambda}^\alpha\mathbf{n} \qquad \Longleftrightarrow \qquad (\dot{\mathbf{S}}_1 - \dot{\mathbf{S}}_2)\mathbf{n} = \mathbf{0}. \tag{46}$$

On substituting this into Eq. (44) and rearranging with the help of Eq. (41), we obtain the relationship

$$\dot f_1^\alpha - \dot f_2^\alpha = -\sum_{\beta\in B} g_{\mathrm{band}}^{\alpha\beta}(\dot\gamma_1^\beta - \dot\gamma_2^\beta) \qquad \forall\alpha\in\mathcal{B}. \tag{47}$$

Assuming that the consistency conditions (5) are satisfied in each band, it follows that

$$(\dot\gamma_1^\alpha - \dot\gamma_2^\alpha)(\dot f_1^\alpha - \dot f_2^\alpha) = -\dot f_2^\alpha\dot\gamma_1^\alpha - \dot f_1^\alpha\dot\gamma_2^\alpha \geq 0\,. \tag{48}$$

Hence, on multiplying Eq. (47) by $(\dot\gamma_1^\alpha - \dot\gamma_2^\alpha)$ (without summation over α), we arrive at a remarkable conclusion that

$$(\dot\gamma_1^\alpha - \dot\gamma_2^\alpha)\sum_{\beta\in B} g_{\mathrm{band}}^{\alpha\beta}(\dot\gamma_1^\beta - \dot\gamma_2^\beta) \leq 0 \qquad \forall\alpha\in\mathcal{B}. \tag{49}$$

In words, inequality (49) means that $g_{\mathrm{band}}^{\mathcal{B}}$ *reverses the sign of the vector* $(\dot\gamma_1^\beta - \dot\gamma_2^\beta)$. By a known mathematical theorem, cf. Cottle et al. (1992, Theorem 3.3.4), fulfilment of the inequality (49) for $(\dot\gamma_1^\beta) \neq (\dot\gamma_2^\beta)$ implies

$$\det g_{\mathrm{band}}^{\mathcal{A}} \leq 0 \qquad \text{for some } \mathcal{A}\subseteq\mathcal{B}\,. \tag{50}$$

Since $\mathcal{B}\subseteq\mathcal{P}$, the derived condition (50) for deformation banding is slightly stronger than violation of the exclusion condition (42) in its basic form. In particular, condition (50) excludes that $g_{\mathrm{band}}^{\mathcal{B}}$ is positive definite.

4.4. The role of latent hardening in deformation pattern formation

So far, in Section 4 we have only used the basic constitutive assumptions given in Section 2.1. To highlight the role of hardening moduli in the conditions (49) and (50) for deformation banding, further constitutive specifications given in Section 2.2 as well as the structure of matrix $(g_{\mathrm{band}}^{\alpha\beta})$ are exploited. From Eqs. (13) and $(41)_1$ it follows that

$$g_{\mathrm{band}}^{\alpha\beta}\dot\gamma_{1\text{-}2}^\beta = (h^{\alpha\beta} + g_{\mathrm{geom}}^{\alpha\beta})\dot\gamma_{1\text{-}2}^\beta - (\boldsymbol{\Lambda}^\alpha\mathbf{n})\cdot\overset{-1}{\mathbf{Q}_{\mathrm{n}}^{\mathrm{e}}}(\boldsymbol{\Lambda}^\beta\mathbf{n})\dot\gamma_{1\text{-}2}^\beta \tag{51}$$

for any numbers $\dot\gamma_{1\text{-}2}^\beta = \dot\gamma_1^\beta - \dot\gamma_2^\beta$.

On writing down the evolution rule (11) for the plastic deformation gradient in each band and taking the difference, we obtain

$$\sum_{\beta\in\mathcal{P}}\mathbf{N}^\beta\dot\gamma_{1\text{-}2}^\beta = (\dot{\mathbf{F}}_1^{\mathrm{p}} - \dot{\mathbf{F}}_2^{\mathrm{p}})\overset{-1}{\mathbf{F}^{\mathrm{p}}}\,. \tag{52}$$

On using Eqs. $(13)_2$ and (52), we obtain

$$\sum_\beta g_{\mathrm{geom}}^{\alpha\beta}\dot\gamma_{1\text{-}2}^\beta = \mathbf{F}^*\mathbf{N}^\alpha\cdot\mathbb{C}^*\cdot\mathbf{F}^*(\dot{\mathbf{F}}_1^{\mathrm{p}} - \dot{\mathbf{F}}_2^{\mathrm{p}})\overset{-1}{\mathbf{F}^{\mathrm{p}}} + \boldsymbol{\Pi}\cdot(\dot{\mathbf{F}}_1^{\mathrm{p}} - \dot{\mathbf{F}}_2^{\mathrm{p}})\overset{-1}{\mathbf{F}^{\mathrm{p}}}\mathbf{N}^\alpha\,. \tag{53}$$

This can be further transformed, using Eqs. $(9)_3$ and (12), as follows:

$$\sum_\beta g_{\mathrm{geom}}^{\alpha\beta}\dot\gamma_{1\text{-}2}^\beta = (\mathbf{F}^*\mathbf{N}^\alpha\cdot\mathbb{C}^* + \overset{\mathrm{T}}{\mathbf{S}^*}\mathbf{N}^\alpha)\cdot\mathbf{F}^*(\dot{\mathbf{F}}_1^{\mathrm{p}} - \dot{\mathbf{F}}_2^{\mathrm{p}})\overset{-1}{\mathbf{F}^{\mathrm{p}}} = \boldsymbol{\Lambda}^\alpha\cdot\mathbf{F}^*(\dot{\mathbf{F}}_1^{\mathrm{p}} - \dot{\mathbf{F}}_2^{\mathrm{p}})\,. \tag{54}$$

From Eqs. $(46)_2$ and $(7)_1$ we have the kinematic relationship

$$\dot{\mathbf{b}}\otimes\mathbf{n} = \dot{\mathbf{F}}_1 - \dot{\mathbf{F}}_2 = \mathbf{F}^*(\dot{\mathbf{F}}_1^{\mathrm{p}} - \dot{\mathbf{F}}_2^{\mathrm{p}}) + (\dot{\mathbf{F}}_1^* - \dot{\mathbf{F}}_2^*)\mathbf{F}^{\mathrm{p}}\,, \tag{55}$$

whose substitution into Eq. (54) yields

$$\sum_\beta g_{\mathrm{geom}}^{\alpha\beta}\dot\gamma_{1\text{-}2}^\beta = -\boldsymbol{\Lambda}^\alpha\cdot(\dot{\mathbf{F}}_1^* - \dot{\mathbf{F}}_2^*)\mathbf{F}^{\mathrm{p}} + \boldsymbol{\Lambda}^\alpha\cdot(\dot{\mathbf{b}}\otimes\mathbf{n})\,. \tag{56}$$

In turn, from the statical compatibility condition $(46)_1$ we have

$$\sum_\beta\boldsymbol{\Lambda}^\beta\mathbf{n}\dot\gamma_{1\text{-}2}^\beta = \mathbf{Q}_{\mathrm{n}}^{\mathrm{e}}\dot{\mathbf{b}}\,. \tag{57}$$

On substituting the expressions (56) and (57) into the formula (51) after summing over β, we obtain

$$\sum_\beta g_{\mathrm{band}}^{\alpha\beta}\dot\gamma_{1\text{-}2}^\beta = \sum_\beta h^{\alpha\beta}\dot\gamma_{1\text{-}2}^\beta - \boldsymbol{\Lambda}^\alpha\cdot(\dot{\mathbf{F}}_1^* - \dot{\mathbf{F}}_2^*)\mathbf{F}^{\mathrm{p}} + \boldsymbol{\Lambda}^\alpha\cdot(\dot{\mathbf{b}}\otimes\mathbf{n}) - (\boldsymbol{\Lambda}^\alpha\mathbf{n})\cdot\dot{\mathbf{b}}\,. \tag{58}$$

The last two terms cancel each other, and we arrive at the useful relationship

$$\sum_{\beta\in B} g_{\mathrm{band}}^{\alpha\beta}\dot\gamma_{1\text{-}2}^\beta = \sum_{\beta\in B} h^{\alpha\beta}\dot\gamma_{1\text{-}2}^\beta - \boldsymbol{\Lambda}^\alpha\cdot(\dot{\mathbf{F}}_1^* - \dot{\mathbf{F}}_2^*)\mathbf{F}^{\mathrm{p}} \qquad \forall\alpha\in\mathcal{B}\,. \tag{59}$$

The particular case of orthogonality of the tensors in the last term (including $\dot{\mathbf{F}}_1^* = \dot{\mathbf{F}}_2^*$) is of special interest, since then

$$\sum_{\beta\in B} g_{\mathrm{band}}^{\alpha\beta}\dot\gamma_{1\text{-}2}^\beta = \sum_{\beta\in B} h^{\alpha\beta}\dot\gamma_{1\text{-}2}^\beta \qquad \text{if } \boldsymbol{\Lambda}^\alpha\cdot(\dot{\mathbf{F}}_1^* - \dot{\mathbf{F}}_2^*)\mathbf{F}^{\mathrm{p}} = 0\,. \tag{60}$$

Then, from equality (47) we obtain

$$\dot f_1^\alpha - \dot f_2^\alpha = -\sum_{\beta\in B} h^{\alpha\beta}(\dot\gamma_1^\beta - \dot\gamma_2^\beta) \qquad \text{if } \boldsymbol{\Lambda}^\alpha\cdot(\dot{\mathbf{F}}_1^* - \dot{\mathbf{F}}_2^*)\mathbf{F}^{\mathrm{p}} = 0 \tag{61}$$

and, if inequality (49) holds, also

$$\dot\gamma_{1\text{-}2}^\alpha\sum_{\beta\in B} h^{\alpha\beta}\dot\gamma_{1\text{-}2}^\beta = \dot\gamma_{1\text{-}2}^\alpha\sum_{\beta\in B} g_{\mathrm{band}}^{\alpha\beta}\dot\gamma_{1\text{-}2}^\beta \leq 0 \qquad \text{if } \boldsymbol{\Lambda}^\alpha\cdot(\dot{\mathbf{F}}_1^* - \dot{\mathbf{F}}_2^*)\mathbf{F}^{\mathrm{p}} = 0\,. \tag{62}$$

This is true $\forall\alpha\in\mathcal{B}$ in the special case of $\dot{\mathbf{F}}_1^* = \dot{\mathbf{F}}_2^*$, and then, in analogy to condition (50), we arrive at the following property of the hardening moduli matrix

$$\det h^{\mathcal{A}} \leq 0 \qquad \text{for some } \mathcal{A}\subseteq\mathcal{B}\,, \qquad h^{\mathcal{A}} = (h^{\alpha\beta}) \text{ with } \alpha,\beta\in\mathcal{A}\,, \tag{63}$$

provided non-negative slip-rates $\dot\gamma_1^\alpha, \dot\gamma_2^\alpha$ satisfy the inequality (48) along with equality $(\dot\gamma_1^\alpha - \dot\gamma_2^\alpha) = (\dot\gamma_{1\text{-}2}^\alpha) \neq (0)$.

For $\dot{\mathbf{F}}_1^* = \dot{\mathbf{F}}_2^*$ to be met for two distinct bands, the following equation

$$\sum_{\beta\in\mathcal{P}}\mathbf{N}^\beta\dot\gamma_{1\text{-}2}^\beta = \overset{-1}{\mathbf{F}^*}\dot{\mathbf{b}}\otimes\overset{-\mathrm{T}}{\mathbf{F}^{\mathrm{p}}}\mathbf{n} \tag{64}$$

must have a solution $(\dot\gamma_{1\text{-}2}^\alpha) \neq (0)$. This equation results from the kinematic relationships (52) and (55). Note that this is only a necessary condition, since the consistency conditions (5) in the bands are not guaranteed, so the associated banding mode (40) is virtual in this sense.

On using Eq. (46) to eliminate vector $\dot{\mathbf{b}}$ from Eq. (64), we arrive at the equation

$$\mathbf{Q}_{\mathrm{n}}^{\mathrm{e}}\mathbf{F}^*\sum_{\alpha\in\mathcal{P}}\mathbf{N}^\alpha\dot\gamma_{1\text{-}2}^\alpha = \sum_{\alpha\in\mathcal{P}}\dot\gamma_{1\text{-}2}^\alpha\boldsymbol{\Lambda}^\alpha\mathbf{n}\otimes\overset{-\mathrm{T}}{\mathbf{F}^{\mathrm{p}}}\mathbf{n}\,, \tag{65}$$

and finally, at

$$\sum_{\alpha\in\mathcal{P}}\mathbf{Z}^\alpha\dot\gamma_{1\text{-}2}^\alpha = \mathbf{0}\,, \qquad \mathbf{Z}^\alpha = \mathbf{Q}_{\mathrm{n}}^{\mathrm{e}}\mathbf{F}^*\mathbf{N}^\alpha - \boldsymbol{\Lambda}^\alpha\mathbf{n}\otimes\overset{-\mathrm{T}}{\mathbf{F}^{\mathrm{p}}}\mathbf{n}\,, \tag{66}$$

for consistency with $\dot{\mathbf{F}}_1^* = \dot{\mathbf{F}}_2^*$.

Once a non-zero vector $(\dot\gamma_{1\text{-}2}^\alpha)$ is found that satisfies Eq. (66), the associated vector $\dot{\mathbf{b}}$ can be determined from Eq. (57) so that all the above equations from (52) onwards are satisfied. In Eq. (66), $\dot\gamma_{1\text{-}2}^\alpha$ are the only unknowns for a given $\mathbf{n}$, and all other quantities are known in a given state from constitutive assumptions.

Hence, we have proven the following statement.

Proposition 2. *Given a homogeneous state and the constitutive assumptions used above, let*

(i) $(\dot\gamma_{1\text{-}2}^\alpha) = (\dot\gamma_1^\alpha - \dot\gamma_2^\alpha) \neq (0)$ *be a solution to Eq. (66) for a given* $\mathbf{n}$*. Then,*

(ii) there exists a virtual deformation banding mode, which satisfies the compatibility conditions (40) across the band interfaces, such that

$$\sum_{\beta\in B} g_{\mathrm{band}}^{\alpha\beta}\dot\gamma_{1\text{-}2}^\beta = \sum_{\beta\in B} h^{\alpha\beta}\dot\gamma_{1\text{-}2}^\beta \qquad \forall\alpha\in\mathcal{B} = \{\alpha\in\mathcal{P} \;:\; \dot\gamma_1^\alpha > 0 \text{ or } \dot\gamma_2^\alpha > 0\}. \tag{67}$$

Table 1
Notation of slip systems, directions and planes in fcc crystals.

$a1$	$a2$	$a3$	$b1$	$b2$	$b3$	$c1$	$c2$	$c3$	$d1$	$d2$	$d3$
$[0\bar{1}1]$	$[10\bar{1}]$	$[\bar{1}10]$	$[011]$	$[\bar{1}0\bar{1}]$	$[1\bar{1}0]$	$[0\bar{1}1]$	$[\bar{1}0\bar{1}]$	$[110]$	$[011]$	$[10\bar{1}]$	$[\bar{1}\bar{1}0]$
	(111)			$(\bar{1}\bar{1}1)$			$(\bar{1}11)$			$(1\bar{1}1)$	

This new result is stronger than that proven as Proposition 3 in Petryk and Kursa (2013). In view of conditional inequality (62), the derived equality (67) highlights the fundamental role played by off-diagonal (latent- or cross-hardening) moduli $h^{\alpha\beta}$ in forming deformation bands in single crystals, at least in the special case $\dot{\mathbf{F}}_1^* = \dot{\mathbf{F}}_2^*$. This is even more clearly visible from the property (63) obtained as a consequence if inequality (48) holds.

If inequality (48) holds for a non-singular matrix $g^{\mathcal{B}}_{\text{band}}$ then inequality (49) must be strict for some α, since $(\dot{\gamma}^{\alpha}_{1\text{-}2}) \neq (0)$. The strict inequality carries over to the sum over $\alpha \in \mathcal{B}$. It can be shown (Petryk and Kursa, 2013, Proposition 2) that the resulting inequality implies the existence of virtual banding modes which are energetically preferable to uniform straining. Since the value of $\Delta_2 w(\Delta\gamma^{\alpha}, \Delta\mathbf{F})$ expressed by Eq. (23) to second-order with respect to Δt is not affected by a skew part of the slip-system interaction matrix, the proof can run on similar lines as before and is therefore omitted here. It can be seen that far reaching conclusions can be drawn from the very existence of a non-zero solution to Eq. (66).

Directions of vectors $(\dot{\gamma}^{\alpha}_1 - \dot{\gamma}^{\alpha}_2)$ and $\dot{\mathbf{b}}$ found by solving Eq. (64) or Eq. (66) for various $\mathbf{n}$ can be taken as good initial guesses in numerical calculations of energetically optimal deformation banding modes. These vectors need to be normalized beforehand because they can only be determined from these equations up to an arbitrary multiplier. Selected normalized solutions to Eq. (64) or Eq. (66) were found helpful in choosing the starting points in the calculations reported below, aimed at solving numerically the minimization problem (38).

5. Numerical examples

5.1. Material properties

Non-symmetric slip-system hardening matrix $(h^{\alpha\beta})$ is specified as follows (Bronkhorst et al., 1992)

$$h^{\alpha\beta} = \left(\chi^{\alpha\beta} + q\left(1 - \chi^{\alpha\beta}\right)\right) h^{\beta}, \tag{68}$$

where the latent-to-self hardening ratio q and coefficients $\chi^{\alpha\beta}$ define latent hardening of the slip systems. Function h^{β} describes the saturation-type hardening in the form

$$h^{\beta} = h_0 \left(1 - \frac{\tau^{\beta}_{\text{cr}}}{\tau_{\text{s}}}\right)^{a} \qquad \text{for } \tau^{\beta}_{\text{cr}} \leq \tau_{\text{s}}\,. \tag{69}$$

Note that generally $h^{\alpha\beta} \neq h^{\beta\alpha}$, unless $\tau^{\alpha}_{\text{cr}} = \tau^{\beta}_{\text{cr}}$ along with $\chi^{\alpha\beta} = \chi^{\beta\alpha}$.

Specific material parameters, $(q, \chi^{\alpha\beta}, h_0, \tau_{\text{s}}, a)$ and elastic constants adopted in the calculations for fcc metal crystals, are given below separately for Cu and Ni in Sections 5.3 and 5.4, respectively.

Standard notation of slip-systems in fcc crystals is given in Table 1, following Taylor (1938a).

5.2. Selected aspects of the quasi-minimization algorithm

The external control need not be fully kinematic. The partial kinematic control is realized by splitting componentwise the deformation gradient tensor into a sum

$$\mathbf{F} = \hat{\mathbf{F}}(\lambda) + \tilde{\mathbf{F}}\,, \qquad \hat{\mathbf{F}}(\lambda) \text{ controlled}\,, \quad \tilde{\mathbf{F}} \text{ free}\,,$$
$$F_{ij} = \begin{cases} \hat{F}_{ij}(\lambda) & \text{if controlled,} \\ \tilde{F}_{ij} & \text{if free}\,. \end{cases} \tag{70}$$

Controlled $\hat{F}_{ij}(\lambda)$ define a deformation program or blocked degrees of freedom. Complementary components $\tilde{F}_{ij}$ of $\tilde{\mathbf{F}}$ are unknown and determined incrementally together with incremental slips $\Delta\gamma^{\alpha}$. An example of partial kinematic control of $\mathbf{F}$ is given in Eq. (71), where free components $\tilde{F}_{ij}$ correspond to zero external stresses.

The problem of quasi-minimization of incremental energy for the simulation of deformation banding using QEP, called *minimization by QEP* for brevity, is defined by the conditions (38) and (39) examined jointly. For this purpose, Δw_i in the left-hand expression (38) has been replaced with the respective incremental energy $\Delta\epsilon_i$; note that Eq. (21) holds true *after* minimization by QEP, but not before. The resulting expression is minimized with respect to parameters $\Delta\gamma^{\alpha}_1, \Delta\gamma^{\alpha}_2, \eta, \mathbf{n}, \Delta\mathbf{b}, \Delta\tilde{\mathbf{F}}$ simultaneously.

In order to study a wide spectrum of banding modes in an initially homogeneous material (although without guarantee of completeness), minimization by QEP was started from a series of predetermined orientations of band normal $\mathbf{n}$. The initial trial orientations $\mathbf{n}_j$ were assumed on the basis of a fixed list of pairs of angles $\{\phi_j, \psi_j\}$ defining the vector orientation $\mathbf{n}_j = (\cos\psi_j \cos\phi_j, \cos\psi_j \sin\phi_j, \sin\psi_j)$. The trial band interfaces were assumed to be parallel to the following families of crystallographic planes: four $\{111\}$, six $\{110\}$, three $\{100\}$ i twelve $\{112\}$, which makes the 25 initial starting points used to find the banding mode. The actual orientation of band interfaces found by incremental work minimization (38) is generally different from the starting point, but may depend on it.

The next key point was to select trial sets $\mathcal{P}_1$, $\mathcal{P}_2$ of potentially active slip systems in the bands, associated with a starting value of vector $\Delta\mathbf{b}$. For this purpose, the set of initial band orientations $\mathbf{n}_j$ was first reduced to those for which Eq. (64) or Eq. (66), transformed to incremental form, had a non-zero solution $(\Delta\gamma^{\alpha}_{1\text{-}2})$. After determining the trial values of $\Delta\gamma^{\alpha}_{1\text{-}2}$, the potentially active slip-systems sets $\mathcal{P}_1$ and $\mathcal{P}_2$ in the bands were estimated as $\mathcal{P}_1 = \{\alpha : \Delta\gamma^{\alpha}_{1\text{-}2} > 0\}$ and $\mathcal{P}_2 = \{\alpha : \Delta\gamma^{\alpha}_{1\text{-}2} < 0\}$. If numbers $\Delta\gamma^{\alpha}_{1\text{-}2}$ had (except null ones) only positive or only negative values, identical trial sets were assumed, $\mathcal{P}_1 = \mathcal{P}_2 = \{\alpha : \Delta\gamma^{\alpha}_{1\text{-}2} > 0 \text{ or } \Delta\gamma^{\alpha}_{1\text{-}2} < 0\}$.

Initial values of volume fraction η was arbitrary assumed as $1/2$. However, in order to check the influence of this initial value on the final results of minimization by QEP, calculations were also performed for $\eta = 1/3$ and $\eta = 2/3$. The obtained final banding modes were then the same as for the initial value equal to $1/2$.

5.3. Simple shear test

If a uniform simple shear activates two slip systems and can be split into two families of *single-slip* bands, then the deformation banding pattern found previously by incremental energy minimization, cf. e.g., Ortiz et al. (2000, Figure 2) or Petryk and Kursa (2013, Figure 3), does not differ from that obtained by minimization by QEP since there is no skew part of matrix $(g^{\alpha\alpha})$ for single slip. In a general case, the skew part of matrix $(g^{\alpha\beta})$ is non-zero and the results are different.

Numerical simulations of a simple shear test were conducted here to analyse the actual experimental test presented in Dmitrieva et al. (2009). Another goal was to compare the results obtained here for the non-symmetric slip-system interaction matrix with the previous ones (Petryk and Kursa, 2013), where the matrix was selectively symmetrized. The modelling of deformation banding during a simple shear test was carried out under kinematic control with a prescribed overall deformation gradient $\bar{\mathbf{F}}(\lambda) = \hat{\mathbf{F}}(\lambda) = \mathbf{1} + \lambda\,\mathbf{M} \otimes \mathbf{N}$ defined by vectors of overall shear direction $\mathbf{M}$ and overall shear plane normal $\mathbf{N}$, and a loading parameter λ. In this case, there are no free components of $\tilde{\mathbf{F}}$. The shear test is designed so that initially the overall shear direction $\mathbf{M}$ is collinear with crystallographic lattice direction $[12\bar{1}]$ and vector $\mathbf{N}$ is collinear with plane normal $(\bar{1}11)$. However, the crystallographic lattice was initially rotated by 5° around the crystallographic direction $[\bar{1}0\bar{1}]$, in order to more accurately simulate the experimentally measured deformation gradient given in Dmitrieva et al. (2009). The

Table 2
Incipient solutions for deformation banding in a simple shear test in the initial step $\lambda \in (0, 10^{-3})$.

Solution	Mode	$\Delta\bar{w}$ [MPa]	η	$\Delta\mathbf{b} \propto$	$\mathbf{n}$	$\mathcal{A}_1$	$\mathcal{A}_2$
#1	Banding	0.0013647	0.5	[101]	$(1\bar{2}1)$	$\{c3, b\bar{1}\}$	$\{b3, c\bar{1}\}$
#2	Banding	0.0013653	0.5	$[\bar{2}12]$	(101)	$\{b3, c3\}$	$\{b\bar{1}, c\bar{1}\}$
#3	Banding	0.0013657	0.5	[101]	$(\bar{1}11)$	$\{b3, c3, b\bar{1}\}$	$\{b3, b\bar{1}, c\bar{1}\}$
#4	Banding	0.0013689	0.25	$[0\bar{1}0]$	$(\bar{1}01)$	$\{b3, b\bar{1}\}$	$\{c3, c\bar{1}\}$
#5	Banding	0.0013728	0.5	$[0\bar{1}0]$	$(\bar{1}01)$	$\{b3, c3, b\bar{1}, c\bar{1}\}$	$\{c3, c\bar{1}\}$
#6	Banding	0.0013738	0.5	[101]	$(\bar{1}\bar{1}1)$	$\{b3, c3, c\bar{1}\}$	$\{c3, b\bar{1}, c\bar{1}\}$
#7	Uniform	0.0013748	None	None	None	$\{b3, c3, b\bar{1}, c\bar{1}\}$	$\{b3, c3, b\bar{1}, c\bar{1}\}$

simulation of the deformation proceeded by increasing the value of loading parameter $\lambda(t)$ from 0 to 0.23 with a constant increment $\Delta\lambda = \Delta t/s$ equal to 10^{-3}.

The material properties for the tested Cu single crystal were adopted as follows. The latent-to-self hardening ratio was taken $q = 1.2$ for all slip-systems, also for coplanar slip-system. The non-symmetric hardening moduli $h^{\alpha\beta}$ were determined from formula (68) with parameters $\chi^{\alpha\beta} = \delta^{\alpha\beta}$, the Kronecker delta. In this work, a different hardening law was used to describe the material behaviour than in the previous work (Petryk and Kursa, 2013), where the power hardening law was used and the moduli matrix $(h^{\alpha\beta})$ was symmetric. As shown below, this change in the hardening description did not significantly affect the results obtained. Saturation-type strain-hardening in the form (69) at room temperature is assumed here, with the initial yield stress $\tau_0 = 1$ MPa, initial hardening parameter $h_0 = 250$ MPa, saturation stress $\tau_s = 144$ MPa and exponent $a = 2$. Constant elastic moduli tensor of the Saint Venant–Kirchhoff model was adopted, with elastic moduli $C_{11} = 170$ GPa, $C_{12} = 124$ GPa, $C_{44} = 75$ GPa taken after Simmons and Wang (1971).

Since the latent hardening parameter q was assumed to be greater than 1 from the outset, the deformation banding was found energetically more favourable than uniform deformation as soon as the plastic strain range was entered. Using the minimization by QEP with multiple starting points as specified in Section 5.2, several solutions with crystal subdivision into bands have been obtained as shown in Table 2. Six different banding solutions, labelled #1 to #6, have been found, and all are initially energetically preferable to solution #7 corresponding to uniform deformation which is given for comparison. Each of the banding solutions corresponds to a different value of the overall incremental work density $\Delta\bar{w}$ in the initial step $\lambda \in (0, \Delta\lambda)$, and solution #1 gives the minimal incremental work at this first step. The incremental work density $\Delta\bar{w}$ in all examples given below has been calculated for constant step size $\Delta\lambda = 10^{-3}$.

However, starting from deformation $\lambda = 0.051$, it is the solution #3 that corresponds to the minimal level of the incremental work $\Delta\bar{w}$, cf. Fig. 2. Solution #3 is thus selected for a more detailed description. From the very beginning of plastic flow, the initially homogeneous crystal splits into two families of deformation bands with equal volume fraction $\eta = 0.5$. The calculated normal vector $\mathbf{n}$ coincides with that of crystallographic plane $(\bar{1}11)$ and initial vector $\Delta\mathbf{b}$ is parallel to crystallographic direction [101]. In the analysed process of deformation, the $\{c3\}$ slip-system is dominant within one family of bands while $\{c\bar{1}\}$ is dominant within the second family. Two secondary slip-systems $\{b\bar{1}, b3\}$ are active in both families of bands. Slip increments $\Delta\gamma^\alpha$ and increments $\Delta\mathbf{b}$ are computed in each discrete step of the deformation process by minimization by QEP. Both $\mathbf{n}$ and η remain unchanged during deformation as soon as banding has been initiated. This simplifying assumption is adopted throughout Section 5.

In Fig. 3, the solution #3 has been compared with the experimental result provided by Dmitrieva et al. (2009) for the shear strain $\lambda = 0.23$. Two families of calculated deformation bands containing active slip-plane traces have been schematically shown in Fig. 3(a) on the side plane (101) of the crystal. The traces of the dominant slip planes are marked in red, and the two traces of the secondary slip in blue, the same in both families. In addition, the lengths of the red and blue traces are proportional to the accumulated shears γ^α on the respective

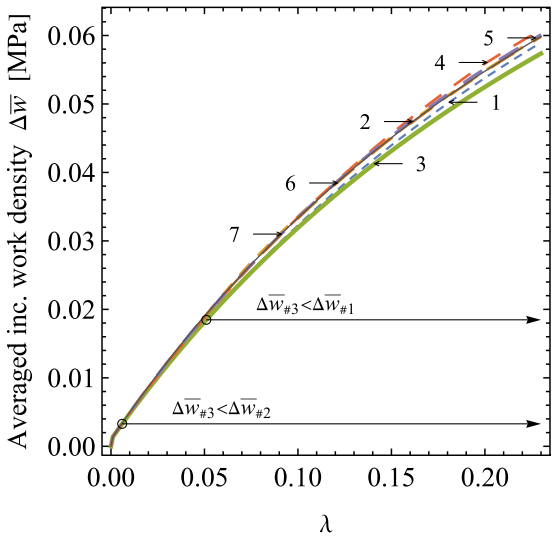

Fig. 2. Comparison of averaged incremental work density $\Delta\bar{w}$ for different solutions with deformation banding, #1 to #6, and for uniform solution #7 during macroscopic simple shear, for $\Delta\lambda = 10^{-3}$.

slip-systems, which shows the quantitative difference in the shear increments on the $\{c\}$ and $\{b\}$ slip-system planes. The calculated angle between the bands and the horizontal side plane of the deformed crystal is 13° and is in agreement with the experimentally calculated value of 12°. The qualitative comparison of experimental and numerical results presented in Fig. 3 is quite satisfactory. The current simulation results are almost the same as in the previous work (Petryk and Kursa, 2013), so in this case, the changes in the hardening law and the extension of the previous minimization of incremental work to the current minimization by QEP did not noticeably affect the results.

5.4. Channel-die compression

The next example of deformation banding in the channel-die compression (CDC) is more complex, although the analysis below is limited to the particular orientation (called cube) of the crystal. For a partial comparison with experiment, we have chosen the experimental results of a detailed analysis provided by Basson and Driver (2000). See also Fathallah et al. (2019) and the references therein for more information about the CDC test.

In order to describe the directions and planes in CDC tests, the commonly used nomenclature has been adopted. Compression is along macroscopic direction X_3 called the normal direction (ND), extension is allowed along direction X_1 called the elongated direction (ED), and deformation is constrained in direction X_2 called the transverse direction (TD) (Fig. 4). For the cube orientation, X_1 = ED = [100], X_2 = TD = [010], and X_3 = ND = [001]. If overall macroscopic shears in this reference frame are negligible then CDC reduces to the plane strain compression.

An overall deformation mode in the channel-die compression test, neglecting the geometric effect of the free ends of the sample, can be

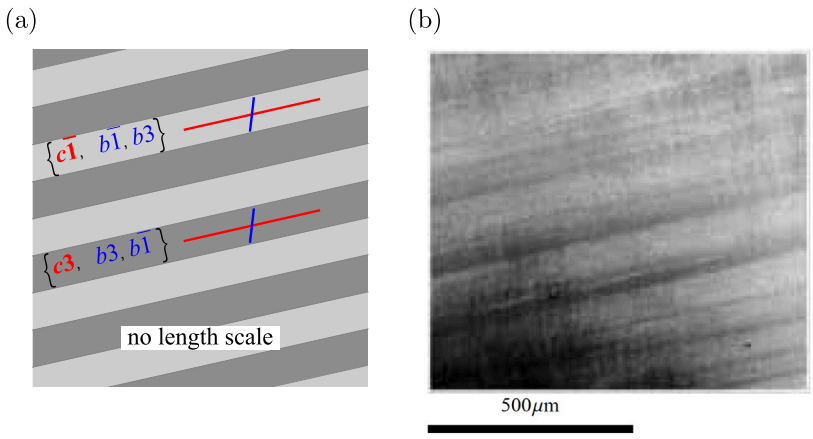

Fig. 3. Simple shear test: (a) Calculated deformation pattern with two families of deformation bands, and slip-plane traces on the side plane (101) of the crystal. The traces of the dominant slip planes are marked in red, and the two traces of the secondary slip in blue, with the lengths of the traces proportional to the accumulated shears on the slip-systems. (b) Deformation bands observed on the side plane of a deformed Cu single crystal, after Dmitrieva et al. (2009). (For interpretation of the references to colour in this figure legend, the reader is referred to the web version of this article.)

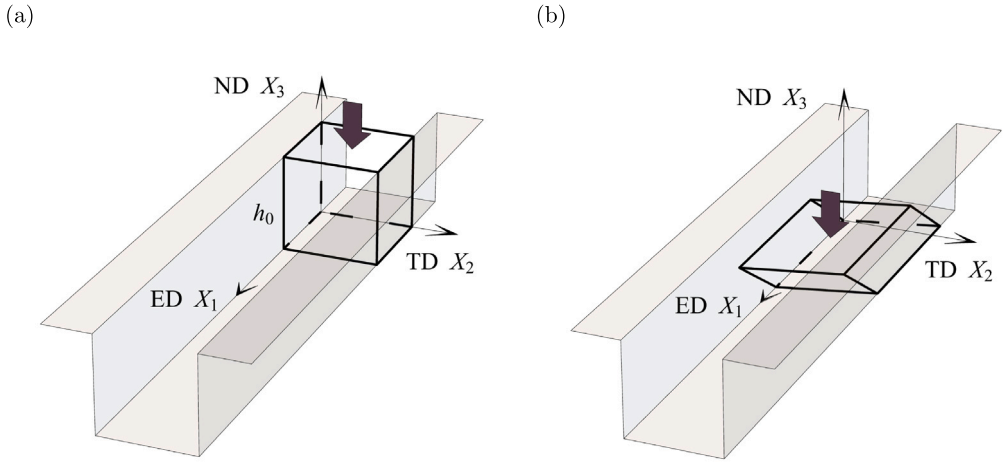

Fig. 4. Schematic view of the channel-die compression test.

simulated by imposing partial constraints on the overall deformation gradient **F** and Piola stress **S** tensors as follows, cf. Eq. (70),

$$\mathbf{F}=\begin{bmatrix}\tilde{F}_{11} & \tilde{F}_{12} & \tilde{F}_{13}\\ 0 & 1 & 0\\ 0 & 0 & 1-\lambda\end{bmatrix},\qquad \mathbf{S}=\begin{bmatrix}0 & 0 & 0\\ \tilde{S}_{12} & \tilde{S}_{22} & \tilde{S}_{23}\\ \tilde{S}_{13} & \tilde{S}_{32} & \tilde{S}_{33}\end{bmatrix}. \tag{71}$$

The compression was kinematically controlled by the prescribed component $\hat{F}_{33}=1-\lambda(t)$, where loading parameter $\lambda(t)$ was changed with a fixed step size $\Delta\lambda=10^{-3}$ starting with $\lambda=0$. Simulations for several tested solutions performed for other step sizes $\Delta\lambda=10^{-4}$ and $\Delta\lambda=10^{-2}$ gave approximately the same results. Unknown components $\tilde{F}_{ij}$ and $\tilde{S}_{ij}$ were determined at each deformation step by the minimization by QEP described above.

Material parameters adopted in the modelling have been set to fit the first part of the experimental equivalent stress–strain curve up to 0.4 of strain, shown in Figure 3(a) in Basson and Driver (2000) for a compressed nickel (Ni) single crystal. Comparison of the experimental and numerical graphs of equivalent stress vs equivalent strain for Ni is shown here in Fig. 5. Saturation-type hardening in the form (69) has been adopted along with initial yield stress $\tau_0=1$ MPa, initial hardening parameter $h_0=500$ MPa, saturation stress $\tau_s=144$ MPa, and $a=2$. The hardening matrix has now two-parameter form with the latent hardening parameter $q=1$ for self-hardening and for coplanar slip-systems, and $q=1.2$ for others, which corresponds to $\chi^{\alpha\beta}=1$ for coplanar systems and 0 otherwise. This is somewhat different from the simple-shear modelling assumption in the previous section. Cubic elastic properties of a Ni single crystal at room temperature are described by elasticity moduli $C_{11}=249$ GPa, $C_{12}=154$ GPa, $C_{44}=122$ GPa, taken as average values in the rows numbered from 11,065 to 11,070 in Simmons and Wang (1971, page 56). An initial orientation $\{100\}\langle001\rangle$ (cube) of a Ni single crystal was taken for the simulation of the channel-die compression test.

A trial set of potentially active slip-systems, e.g., defined as $\mathcal{P}=\mathcal{A}_n\cup\{\alpha|f^\alpha_{\rm tr}>\epsilon\}$ in the notation of Petryk and Kursa (2022), for the initial time step $\Delta\lambda=10^{-3}$ consists of twelve systems $\mathcal{P}=\{a2,b2,c2,d2,a\bar{1},a\bar{3},b\bar{1},b\bar{3},c\bar{1},c\bar{3},d\bar{1},d\bar{3}\}$. Three groups of potentially active systems can be distinguished according to their overload level. The most and equally stressed are four slip-systems $\{a2,b2,c2,d2\}$, the next four are $\{a\bar{1},b\bar{1},c\bar{1},d\bar{1}\}$ and the next are $\{a\bar{3},b\bar{3},c\bar{3},d\bar{3}\}$. The threshold resolved shear stress is initially exceeded for these twelve trial systems for deformation steps $10^{-2},10^{-3},10^{-4}$, while for the smaller step 10^{-5} this trial set reduces to the four listed above as the most stressed. As before, since the latent hardening parameter $q>1$ from the beginning, the deformation banding is found energetically more favourable than uniform deformation as soon as the plastic strain range has been entered.

5.4.1. *Results for constrained* $\hat{F}_{12}=0$ *and* $\Delta\mathbf{b}\propto[1\,0\,0]$

In order to reflect the real experimental conditions of the test, we suppose first that the friction on the lateral surfaces of the channel

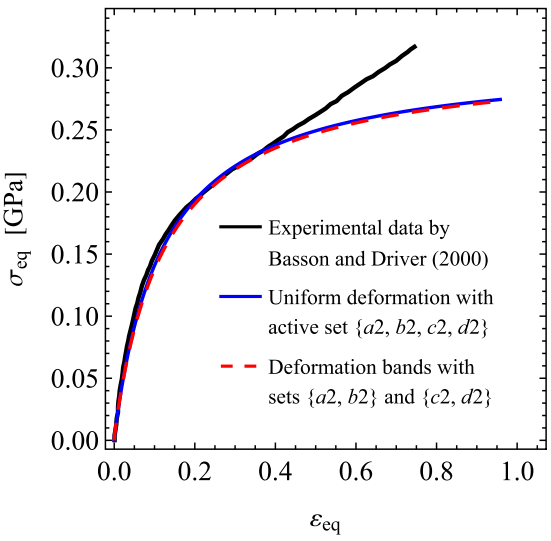

Fig. 5. Comparison of the experimental and numerical graphs of equivalent stress vs equivalent strain for a Ni single crystal. The thick black line represents the experimental curve obtained from the channel-die test by Basson and Driver (2000). The solid blue curve is for the simulation of uniform deformation with four active slip systems $\mathcal{A} = \{a2, b2, c2, d2\}$. The dashed red curve is for a non-uniform solution with two families of bands with active slip systems $\mathcal{A}_1 = \{a2, b2\}$ and $\mathcal{A}_2 = \{c2, d2\}$, described in Section 5.4.1. (For interpretation of the references to colour in this figure legend, the reader is referred to the web version of this article.)

prevents overall deformation F_{12}. Therefore, we take here $\hat{F}_{12} = 0$ instead of arbitrary $\tilde{F}_{12}$, but deformation $\tilde{F}_{13} \neq 0$ is allowed.

In the first approach used in this subsection, it is assumed that the unknown vector $\Delta\mathbf{b}$ has a direction along X_1 (ED), so it corresponds to direction [1 0 0] of the crystallographic lattice. This direction is the only one which does not cross the channel boundaries, which motivated its choice. It has been checked that for the incipient deformation banding mode $(\dot{\mathbf{b}}, \mathbf{n})$ corresponding to $([1\,0\,0], (0\,1\,0))$, there exists a solution $(\dot{\gamma}^{\alpha}_{1\text{-}2}) \neq (0)$ to Eq. (64). Under this assumption and using multiple starting points as specified in Section 5.2, as a result of the simulation only one type of solution has been found, which corresponds to the splitting of the crystal into deformation bands with the sets $\mathcal{A}_1 = \{a2, b2\}$ and $\mathcal{A}_2 = \{c2, d2\}$ of active slip-systems. The initially calculated volume fraction of the bands is $\eta = 0.5$ and remains constant in subsequent deformation steps. The band interface is coplanar with the crystallographic plane (0 1 0) parallel to the ED-ND plane. In this case, the deformation proceeds without crystallographic lattice rotation. The calculated active slip-plane traces on the compression face, Fig. 6(a, b), are in satisfactory agreement with the experimental pattern shown in Fig. 6(c) after Basson and Driver (2000) for compressive logarithmic strain $\epsilon = 0.83$. The lower band in Fig. 6(a) contains slip-planes traces of two active slip-systems $\mathcal{A}_1 = \{a2, b2\}$, while the upper band contains traces of active slip-systems $\mathcal{A}_2 = \{c2, d2\}$.

5.4.2. Results for constrained $\hat{F}_{12} = 0$ and free $\Delta\mathbf{b}$

In the second approach presented here, the calculations of deformation banding are still performed for $\hat{F}_{12} = 0$ but now for unconstrained direction of vector $\Delta\mathbf{b}$. In this case, several solutions are available already in the initial step $(0, \Delta\lambda)$, see Table 3. All the solutions found either split the crystal into two families of bands of volume fraction $\eta = 0.5$ or correspond to uniform deformation.

Due to the symmetry of loading with respect to the crystallographic lattice, the following alternative and energetically equivalent solutions to $\#1_a$, $\#2_a$ and $\#3_a$ were found in the calculations, which are available but not included in Table 3:

Alternative to $\#1_a$: $\eta = 0.5$, $\Delta\mathbf{b} \propto [101]$, $\mathbf{n} = (010)$, $\mathcal{A}_1 = \{b2\}$, $\mathcal{A}_2 = \{c2\}$.

Alternative to $\#2_a$: $\eta = 0.5$, $\Delta\mathbf{b} \propto [010]$, $\mathbf{n} = (101)$, $\mathcal{A}_1 = \{b2\}$, $\mathcal{A}_2 = \{c2\}$.

Alternative to $\#3_a$: $\eta = 0.5$, $\Delta\mathbf{b} \propto [001]$, $\mathbf{n} = (010)$, $\mathcal{A}_1 = \{b2, d2\}$, $\mathcal{A}_2 = \{a2, c2\}$.

The solution labelled $\#3_a$ coincides with that found in Section 5.4.1 above and illustrated in Fig. 6(a, b). The solutions in Table 3 have been sorted according to the increasing initial value of $\Delta\bar{w}$. Comparison of the averaged incremental work density $\Delta\bar{w}$ (which for constant step size $\Delta\lambda$ reduces to comparison of nominal stress $|S_{33}| \approx \Delta\bar{w}/\Delta\lambda$) corresponding to the continuation of these solutions during subsequent deformation is presented in Fig. 7.

The changes of active slip systems along the deformation paths initiated by different solutions as in Table 3 are given in Table 4. For banded solution $\#3_a$ and for uniform solution $\#5_a$, there are no changes of active slip-systems until the final deformation at $\lambda = 0.41$. The changes of active slip-systems were detected automatically in the course of deformation by the incremental minimization by QEP.

The solutions that correspond to the smallest work expenditure at the initial stage, namely $\#1_a$ and $\#2_a$ as it is visible in Table 3, are no longer energetically preferred at a later stage. Finally, it is the solution $\#3_a$ that gives the smallest increase in the deformation work during deformation, cf. Fig. 7. Recall that solution $\#3_a$ found for unconstrained $\Delta\mathbf{b}$ is equivalent to the solution found in Section 5.4.1 assuming $\Delta\mathbf{b} \propto [1\,0\,0]$, illustrated in Fig. 6(a, b).

5.4.3. Results for free $\tilde{F}_{12}$ and free $\Delta\mathbf{b}$

In the third approach, the constraint imposed above on $\tilde{F}_{12}$ is removed, and the solutions for deformation banding during channel-die compression are calculated by imposing partial constraints on the overall deformation gradient $\mathbf{F}$ and Piola stress $\mathbf{S}$ in the general form (71).

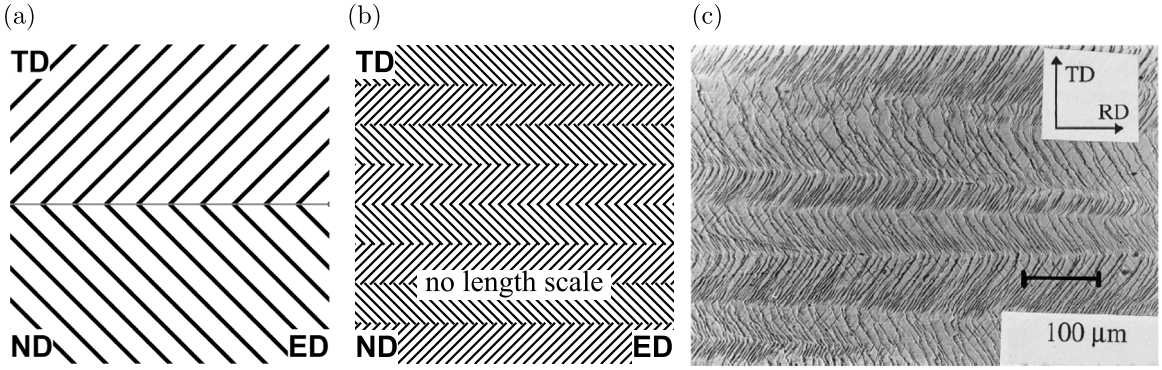

Fig. 6. Plane strain compression: (a) calculated slip-plane traces of dominant slip-systems, $\mathcal{A}_1 = \{a2, b2\}$ in the lower band and $\mathcal{A}_2 = \{c2, d2\}$ in the upper band, (b) herring-bone pattern of traces within two families of deformation bands, (c) the observed pattern of slip traces on the compression face for a cube-oriented Ni crystal at compressive strain $\epsilon = 0.83$, after Basson and Driver (2000).

Table 3
Incipient solutions for deformation banding in channel-die compression for $\hat{F}_{12} = 0$ and free $\Delta\mathbf{b}$ in the initial step $(0, 10^{-3})$.

Solution	Mode	$\Delta\bar{w}$ [MPa]	η	$\Delta\mathbf{b} \propto$	$\mathbf{n}$	$\mathcal{A}_1$	$\mathcal{A}_2$
$\#1_a$	Banding	0.0038179	0.5	$[\bar{1}01]$	(010)	$\{d2\}$	$\{a2\}$
$\#2_a$	Banding	0.0038180	0.5	[010]	$(\bar{1}01)$	$\{d2\}$	$\{a2\}$
$\#3_a$	Banding	0.0039514	0.5	[100]	(010)	$\{a2, b2\}$	$\{c2, d2\}$
$\#4_a$	Uniform	0.0039514	None	None	None	$\{b2, c2\}$	$\{b2, c2\}$
$\#5_a$	Uniform	0.0040178	None	None	None	$\{a2, b2, c2, d2\}$	$\{a2, b2, c2, d2\}$

Table 4
Changes of active slip-systems in the bands up to final deformation $\lambda = 0.41$ during channel-die compression with $\hat{F}_{12} = 0$ and free $\Delta\mathbf{b}$, for banded solutions $\#1_a$, $\#2_a$ and uniform solution $\#4_a$, initiated as in Table 3. For solutions $\#3_a$ and $\#5_a$ there were no further changes of active slip-systems.

Solution $\#1_a$ with banding

λ	$\mathcal{A}_1$	$\mathcal{A}_2$
0.001	$\{d2\}$	$\{a2\}$
0.354	$\{d2, d\bar{1}\}$	$\{a2, a\bar{1}\}$

Solution $\#2_a$ with banding

λ	$\mathcal{A}_1$	$\mathcal{A}_2$
0.001	$\{d2\}$	$\{a2\}$
0.002	$\{b2, d2\}$	$\{a2, c2\}$
0.013	$\{b2, d2, d\bar{3}\}$	$\{a2, c2, a\bar{3}\}$
0.093	$\{a2, b2, d2\}$	$\{a2, c2, d2\}$
0.220	$\{a2, b2, d2, b\bar{3}\}$	$\{a2, c2, d2, a\bar{3}\}$
0.259	$\{b2, d2, b\bar{3}\}$	$\{a2, c2, a\bar{3}\}$

Solution $\#4_a$ – uniform

λ	$\mathcal{A}$
0.001	$\{b2, c2\}$
0.354	$\{b2, c2, b\bar{1}, c\bar{1}\}$

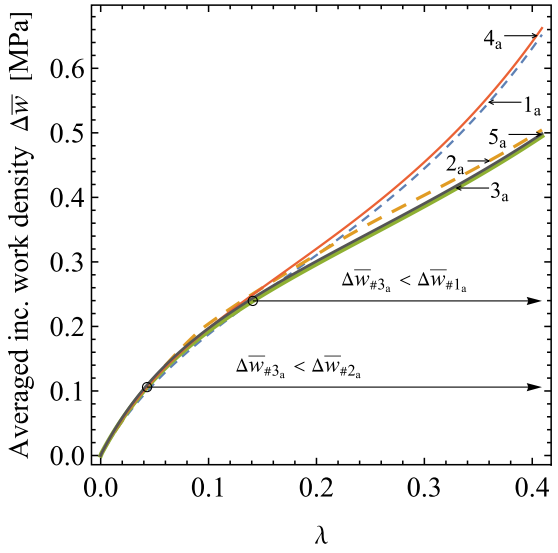

Fig. 7. Comparison of averaged incremental work density $\Delta\bar{w}$ for banded solutions $\#1_a$ to $\#3_a$ and for uniform solutions $\#4_a$ and $\#5_a$ (numbered as in Table 3) during channel-die compression for $\hat{F}_{12} = 0$ and free $\Delta\mathbf{b}$, for $\Delta\lambda = 10^{-3}$.

Unknown increment $\Delta\mathbf{b}$ is here also unconstrained. This type of analysis can be interpreted as the search for secondary banding modes within the primary bands defined by solution $\#3_a$ above. This is because each band interface of orientation $\mathbf{n} = (010)$ in solution $\#3_a$ is parallel to the lateral boundaries of the channel die and is subject to the same boundary conditions in the absence of friction.

A number of different solutions collected in Table 5 are available is this case in the initial deformation step. Similarly as before, because of the symmetry of loading with respect to the crystallographic lattice, there are alternative and energetically equivalent solutions to the solutions $\#1_b$ to $\#4_b$ which are not included in Table 5:

Alternative to $\#1_b$: $\eta = 0.5$, $\Delta\mathbf{b} \propto [010]$, $\mathbf{n} = (001)$, $\mathcal{A}_1 = \{d2\}$, $\mathcal{A}_2 = \{c2\}$.

Alternative to $\#2_b$: $\eta = 0.5$, $\Delta\mathbf{b} \propto [\bar{1}0\bar{1}]$, $\mathbf{n} = (0\bar{1}0)$, $\mathcal{A}_1 = \{b2\}$, $\mathcal{A}_2 = \{c2\}$.

Table 5
Incipient solutions for deformation banding in channel-die compression with free $\hat{F}_{12}$ and free $\Delta\mathbf{b}$.

Solution	Mode	$\Delta\bar{w}$ [MPa]	η	$\Delta\mathbf{b} \propto$	$\mathbf{n}$	$\mathcal{A}_1$	$\mathcal{A}_2$
$\#1_b$	Banding	0.0038157	0.5	[010]	$(00\bar{1})$	$\{a2\}$	$\{b2\}$
$\#2_b$	Banding	0.0038179	0.5	$[10\bar{1}]$	$(0\bar{1}0)$	$\{d2\}$	$\{a2\}$
$\#3_b$	Banding	0.0038180	0.5	$[0\bar{1}0]$	$(\bar{1}0\bar{1})$	$\{b2\}$	$\{c2\}$
$\#4_b$	Banding	0.0038184	0.5	[001]	(010)	$\{b2\}$	$\{a2\}$
$\#5_b$	Uniform	0.0039514	None	None	None	$\{b2, c2\}$	$\{b2, c2\}$
$\#6_b$	Banding	0.0039517	0.5	$[0\bar{1}0]$	(100)	$\{a2, d2\}$	$\{a2, b2\}$

Table 6
Changes of active slip-systems in the bands up to final deformation $\lambda = 0.41$ during channel-die compression with free $\hat{F}_{12}$ and free $\Delta\mathbf{b}$, for banded solutions $\#1_b$, $\#3_b$ and $\#4_b$ initiated as in Table 5.

Solution $\#1_b$ with banding

λ	$\mathcal{A}_1$	$\mathcal{A}_2$
0.001	$\{a2\}$	$\{b2\}$
0.027	$\{a2, a\bar{3}\}$	$\{b2, b\bar{3}\}$
0.098	$\{a2, b\bar{3}\}$	$\{b2, a\bar{3}\}$
0.192	$\{a2, c\bar{3}\}$	$\{b2, d\bar{3}\}$

Solution $\#3_b$ with banding

λ	$\mathcal{A}_1$	$\mathcal{A}_2$
0.001	$\{b2\}$	$\{c2\}$
0.002	$\{b2\}$	$\{a2, c2\}$
0.013	$\{b2, b\bar{3}\}$	$\{a2, c2, c\bar{3}\}$
0.061	$\{b2, b\bar{3}, d\bar{3}\}$	$\{a2, b2, c2, c\bar{3}\}$
0.117	$\{b2, a\bar{3}\}$	$\{a2, b2, c2\}$
0.353	$\{b2, a\bar{3}, d\bar{3}\}$	$\{a2, b2, c2, c\bar{3}\}$
0.368	$\{b2, d\bar{3}\}$	$\{a2, c2, c\bar{3}\}$

Solution $\#4_b$ with banding

λ	$\mathcal{A}_1$	$\mathcal{A}_2$
0.001	$\{b2\}$	$\{a2\}$
0.006	$\{b2, b\bar{1}\}$	$\{a2, a\bar{1}\}$
0.01	$\{b2, a\bar{3}, b\bar{1}, d\bar{3}\}$	$\{a2, a\bar{1}, c\bar{3}\}$

Alternative to $\#3_b$: $\eta = 0.5$, $\Delta\mathbf{b} \propto [010]$, $\mathbf{n} = (\bar{1}01)$, $\mathcal{A}_1 = \{d2\}$, $\mathcal{A}_2 = \{a2\}$.

Alternative to $\#4_b$: $\eta = 0.5$, $\Delta\mathbf{b} \propto [00\bar{1}]$, $\mathbf{n} = (010)$, $\mathcal{A}_1 = \{c2\}$, $\mathcal{A}_2 = \{d2\}$.

As before, the incipient solutions in Table 5 have been sorted according to the increasing initial value of $\Delta\bar{w}$. Comparison of the averaged incremental work density $\Delta\bar{w}$ during subsequent deformation is presented in Fig. 8. The solution $\#3_b$ is energetically preferred at a later stage of deformation, it finally gives the smallest increase in the deformation work, cf. Fig. 8.

The changes of active slip systems along the deformation paths initiated by three solutions from Table 5 are given in Table 6. The banded solution $\#2_b$ shown in Table 5 is the same as solution $\#1_a$ in Table 3, and uniform solution $\#5_b$ shown in Table 5 is the same as solution $\#4_a$ in Table 3. The changes of active slip systems in these two solutions are the same as in Table 4. Note that no solution corresponding to $\#3_a$ appears in Table 5, probably because this solution in the initial step no longer represents a minimum when the previous constraint $\hat{F}_{12} = 0$ has been relaxed.

5.4.4. Discussion

Geometrically exact analysis of deformation banding during the channel-die compression (CDC) of a cube-oriented fcc single crystal turned out to be quite complex. A number of different solutions have been calculated, the experimental validation or invalidation of which is not an easy task. Nevertheless, the proposed method of simulating deformation bands by quasi-minimization of the incremental energy using QEP (*minimization by QEP*), defined by the conditions (38) and

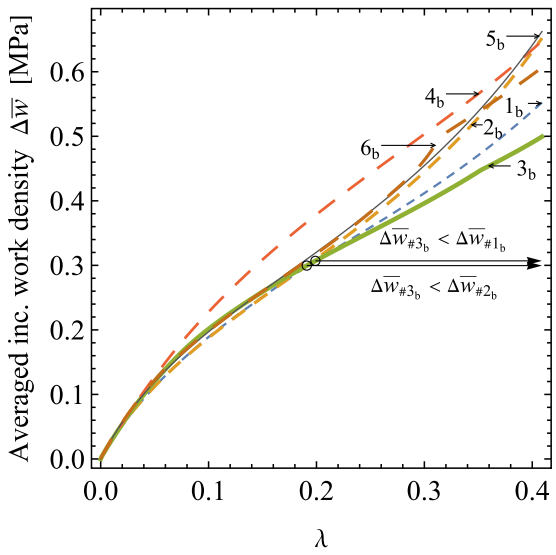

Fig. 8. Comparison of averaged incremental work density $\Delta\bar{w}$ in deformation bands initiated by solutions $\#1_b$ to $\#4_b$ and $\#6_b$ in Table 5, and for uniform deformation $\#5_b$, during channel-die compression with free $\tilde{F}_{12}$ and free $\Delta\mathbf{b}$, for $\Delta\lambda = 10^{-3}$.

(39), has provided an effective tool for a thorough analysis of the different deformation banding modes.

The multiplicity of solutions shown in Tables 3 and 5 is qualitatively similar to experimental results, where differently oriented bands of deformation can be seen (Basson and Driver, 2000). A kind of difficulty in the modelling is in choosing the solution that best describes the experiment. Selected solutions in Sections 5.4.2 and 5.4.3, labelled as $\#3_a$ and $\#3_b$, initially do not give the smallest increase in energy. Only at a later stage of deformation, cf. Figs. 7 and 8, they give the smallest work increments among other solutions. In agreement with experimental observations in Basson and Driver (2000), cf. Fig. 6, it can be concluded that the solution $\#3_a$ correctly describes the formation of *primary* deformation bands. The immediate splitting of each primary band into *secondary* bands is predicted by solution $\#1_b$ and its equivalent alternative. Additionally, several solutions given in Tables 3 and 5 offer other possibilities of the description of secondary bands with single slip. Comparing the solutions for CDC test in the previous subsections, it can be seen that the obtained solutions, both initial and final, are strongly influenced by the assumed boundary conditions and unknown direction $\Delta\mathbf{b}$.

Another difficulty in the modelling of CDC comes from the friction on the channel boundaries that can occur in an experimental test. In order to take friction into consideration at least indirectly in the numerical simulations, we have imposed extra conditions by zeroing selected degrees of freedom, i.e., the deformation gradient component $\hat{F}_{12} = 0$. This assumption has had a significant impact on the obtained solutions, since in the case of modelling where component $\tilde{F}_{12}$ is free, the minimization by QEP gives other possible solutions, cf. Table 5.

In all cases examined, the deformation banding was found energetically more favourable than uniform deformation as soon as the plastic strain range was entered. This is because the latent hardening parameter q was assumed from the beginning to be greater than 1, which opened the possibility that the key matrix g_{band} would be indefinite and the banding modes would be energetically favoured over uniform straining, see Section 4.4. This is in contrast to the experimental observations by Basson and Driver (2000), where the deformation bands were observed at a later stage of the deformation and not from the very beginning. To reconcile different observations, the commonly accepted assumption that the value of the latent-to-self-hardening ratio is constant in the plastic range may be reconsidered in further work. In view of small differences in the calculates values of $\Delta\bar{w}$ for different solutions, it cannot be ruled out that other factors neglected here (like interfacial energy) may prevent early banding, which can be included in future studies.

6. Conclusion

The incremental work criterion (38) for the onset of deformation banding has been combined with the quasi-extremal energy principle (29) for determining the active slip systems and slip increments in the bands in a single crystal with a non-symmetric slip-system interaction matrix. For the first time, the non-potential incremental problem of deformation banding has been addressed by energy minimization in full accordance with the classical constitutive framework of rate-independent crystal plasticity in its general form, established by Hill and Rice (1972). The theoretical analysis revealed the intuitively expected but usually not mathematically explicit role of latent hardening in deformation pattern formation, at least in the particular case when the conditional inequality (62) is satisfied. The common assumption that the latent hardening parameter q has a constant value greater than one in the entire range of plastic deformation turned out to be too strong to explain deformation banding only after the initial period of uniform plastic strain.

In the numerical examples presented in Section 5, more than one local (quasi-)minimum of the total energy expression was found, which corresponds to multiple solutions to the incremental problem of deformation band formation. The solution corresponding to the initially lowest energy increment is not necessarily the most physically significant, so that it is a non-trivial task to solve the deformation banding problem in a satisfactory manner. By considering work expenditure in a longer interval of the external strain parameter, some features of the deformation band geometry were correctly captured. Further work in this direction is needed, as without good predictions of the phenomenon of deformation banding observed for decades, a model of crystal plasticity can hardly be regarded as experimentally validated.

Declaration of competing interest

The authors declare that they have no known competing financial interests or personal relationships that could have appeared to influence the work reported in this paper.

Data availability

Data will be made available on request

Acknowledgements

The presented research did not receive any specific grant from funding agencies in the public, commercial, or not-for-profit sectors.

References

Anand, L., Kalidindi, S.R., 1994. The process of shear band formation in plane strain compression of fcc metals: Effects of crystallographic texture. Mech. Mater 17, 223–243.
Anguige, K., Dondl, P., Kružík, M., 2018. On the existence of minimisers for strain-gradient single-crystal plasticity. ZAMM - J. Appl. Math. Mech. Z. Angew. Math. Mech. 98, 431–447.
Asaro, R.J., 1983. Micromechanics of crystals and polycrystals. Adv. Appl. Mech. 23, 1–115.
Ball, J.M., 1977. Convexity conditions and existence theorems in nonlinear elasticity. Arch. Ration. Mech. Anal. 63, 337–403.
Barrett, C.S., Levenson, L.H., 1939. Structure of iron after drawing, swaging and elongation in tension. Trans. AIME 135, 327–352.
Bassani, J.L., 1994. Plastic flow of crystals. Adv. Appl. Mech. 30, 191–258.
Basson, F., Driver, J.H., 2000. Deformation banding mechanisms during plane strain compression of cube-oriented f.c.c. Crystals. Acta Mater. 48, 2101–2115.
Bay, B., Hansen, N., Hughes, D.A., Kuhlmann-Wilsdorf, D., 1992. Evolution of f.c.c, deformation structures in polyslip. Acta Metall. Mater. 40, 205–219.

Bay, B., Hansen, N., Kuhlmann-Wilsdorf, D., 1989. Deformation structures in lightly rolled pure aluminium. Mater. Sci. Eng. A 113, 385–397.
Bertsekas, D.P., 1996. Constrained Optimization and Lagrange Multiplier Methods, second ed. Athena Scientific, Belmont, Massachustestts.
Bigoni, D., 2012. Nonlinear Solid Mechanics: Bifurcation Theory and Material Instability. Cambridge University Press.
Bronkhorst, C.A., Kalidindi, S.R., Anand, L., 1992. Polycrystalline plasticity and the evolution of crystallographic texture in FCC metals. Philos. Trans. R. Soc. Lond. A Math. Phys. Eng. Sci. 341, 443–477.
Butler, G.C., Stock, S.R., McGinty, R.D., McDowell, D.L., 2002. X-ray microbeam Laue pattern studies of the spreading of orientation in OFHC copper at large strains. J. Eng. Mater. Technol. 124, 48–54.
Carstensen, C., Conti, S., Orlando, A., 2008. Mixed analytical-numerical relaxation in finite single-slip crystal plasticity. Continuum Mech. Thermodyn. 20, 275–301.
Carstensen, C., Hackl, K., Mielke, A., 2002. Non-convex potentials and microstructures in finite-strain plasticity. Proc. R. Soc. Lond. Ser. A Math. Phys. Eng. Sci. 458, 299–317.
Chin, G.Y., Wonsiewicz, B.C., 1969. Deformation banding and stability of (100)-(111) fiber textures of fcc metals. Trans. Metall. Soc. AIME 245 (871).
Chipot, M., Kinderlehrer, D., 1988. Equilibrium configurations of crystals. Arch. Ration. Mech. Anal. 103, 237–277.
Conti, S., Theil, F., 2005. Single-slip elastoplastic microstructures. Arch. Ration. Mech. Anal. 178, 125–148.
Cottle, R.W., Pang, J.S., Stone, R.E., 1992. The Linear Complementarity Problem. Academic Press Inc., San Diego.
Cuitiño, A.M., Ortiz, M., 1993. Computational modelling of single crystals. Model. Simul. Mater. Sci. Eng. 1, 225–263.
de Souza Neto, E.A., Perić, D., Owen, D.R.J., 2008. Computational Methods for Plasticity: Theory and Applications. John Wiley & Sons Ltd, Chichester, UK.
Dequiedt, J., 2018. The incidence of slip system interactions on the deformation of FCC single crystals: System selection and segregation for local and non-local constitutive behavior. Int. J. Sol. Struct. 141-142, 1–14.
Dequiedt, J., 2019. Selection of slip systems in confined single crystal gradient plasticity: Coupled effects of slip system orientations, latent hardening, and grain boundaries. Arch. Mech. 71, 207–238.
Dequiedt, J., 2021. Slip system activity in gradient enhanced crystal plasticity: Grain boundary modelling and bi-crystal response. Int. J. Solids Struct. 225, 111057.
Dmitrieva, O., Dondl, P.W., Müller, D., 2009. Lamination microstructure in shear deformed copper single crystals. Acta Mater. 57, 3439–3449.
Erdle, H., Böhlke, T., 2017. A gradient crystal plasticity theory for large deformations with a discontinuous accumulated plastic slip. Comp. Mech. 60, 923–942.
Fathallah, K., Chenaoui, A., Darrieulat, M., Dogui, A., 2019. Material rotating frame, rate-independent plasticity with regularization of Schmid law and study of channel-die compression. Math. Mech. Solids 24, 18–39.
Franciosi, P., Zaoui, A., 1991. Crystal hardening and the issue of uniqueness. Int. J. Plast. 7, 295–311.
Giarola, D., Capuani, D., Bigoni, D., 2018. Dynamic interaction of multiple shear bands. Sci. Rep. 8 (16033).
Hansen, B.L., Bronkhorst, C.A., Ortiz, M., 2010. Dislocation subgrain structures and modeling the plastic hardening of metallic single crystals. Model. Simul. Mater. Sci. Eng. 18, 055001.
Havner, K.S., 1992. Finite Plastic Deformation of Crystalline Solids. Cambridge University Press, Cambridge.
Hill, R., 1978. Aspects of invariance in solids mechanics. Adv. Appl. Mech. 18, 1–75.
Hill, R., Rice, J.R., 1972. Constitutive analysis of elastic–plastic crystals at arbitrary strain. J. Mech. Phys. Solids 20, 401–413.
Homayonifar, M., Mosler, J., 2011. On the coupling of plastic slip and deformation-induced twinning in magnesium: A variationally consistent approach based on energy minimization. Int. J. Plast. 27, 983–1003.
Honeycombe, R.W.K., 1951. Inhomogeneities in the plastic deformation of metal crystals. 2. X-Ray and optical micrography of aluminium. J. Inst. Metals 80, 49–56.
Huang, X., Hansen, N., 1997. Grain orientation dependence of micorstructure in aluminium deformed in tension. Scr. Mater. 37, 1–7.
Huang, X., Winther, G., 2007. Dislocation structures. Part I. Grain orientation dependence. . Phil. Mag 87, 5189–5214.
Hughes, D.A., Liu, Q., Chrzan, D.C., Hansen, N., 1997. Scaling of microstructural parameters: Misorientations of deformation induced boundaries. Acta Mater. 45, 105–112.
Klusemann, B., Kochmann, D.M., 2014. Microstructural pattern formation in finite-deformation single-slip crystal plasticity under cyclic loading: Relaxation vs. gradient plasticity. Comp. Meth. Appl. Mech. Engng 278, 765–793.
Kochmann, D.M., Hackl, K., 2011. The evolution of laminates in finite crystal plasticity: a variational approach. Continuum Mech. Thermodyn. 23, 63–85.
Kratochvíl, J., Kružík, M., Sedláček, R., 2010. Instability origin of subgrain formation in plastically deformed materials. Int. J. Engng. Sci. 48, 1401–1412.
Kröner, E., 1960. Allgemeine kontinuumstheorie der versetzungen und eigenspannungen. Arch. Ration. Mech. Anal. 4, 273–334.
Kuhlmann-Wilsdorf, D., 1999. "Regular" deformation bands (DBs) and the LEDS hypothesis. Acta Mater. 47, 1697–1712.
Kuhlmann-Wilsdorf, D., Kulkarni, S.S., Moore, J.T., Starke, Jr., E.A., 1999. Deformation bands, the LEDS theory, and their importance in texture development: Part I. Previous evidence and new observations. Metall. Mater. Trans. A 30, 2491–2501.
Kumar, S., Vidyasagar, A., Kochmann, D.M., 2020. An assessment of numerical techniques to find energy-minimizing microstructures associated with nonconvex potentials. Int. J. Num. Meth. Engng. 121, 1595–1628.
Kuroda, M., Tvergaard, V., 2006. Studies of scale dependent crystal viscoplasticity models. J. Mech. Phys. Solids 54, 1789–1810.
Kuroda, M., Tvergaard, V., 2008. A finite deformation theory of higher-order gradient crystal plasticity. J. Mech. Phys. Solids 56, 2573–2584.
Lebensohn, R., Tomé, C., 1993. A self-consistent anisotropic approach for the simulation of plastic deformation and texture development of polycrystals: Application to zirconium alloys. Acta Metall. Mater. 41, 2611–2624.
Lee, C.S., Duggan, B.J., 1993. Deformation banding and copper-type rolling textures. Acta Metall. Mater. 41, 2691–2699.
Lee, C.S., Duggan, B.J., Smallman, R.E., 1993. A theory of deformation banding in cold rolling. Acta Metall. Mater. 41, 2265–2270.
Lewandowski, M., Stupkiewicz, S., 2018. Size effects in wedge indentation predicted by a gradient-enhanced crystal-plasticity model. Int. J. Plast. 109, 54–78.
Luan, Q., Xing, H., Zhang, J., Jiang, J., 2020. Experimental and crystal plasticity study on deformation bands in single crystal and multi-crystal pure aluminium. Acta Mater. 183, 78–92.
Madec, R., Kubin, L.P., 2017. Dislocation strengthening in FCC metals and in BCC metals at high temperatures. Acta Mater. 126, 166–173.
Mandel, J., 1971. Plasticité Classique Et Viscoplasticité. In: CISM Courses and Lectures, vol. 97, Springer-Verlag, Wien-New York.
Miehe, C., Lambrecht, M., Gürses, E., 2004. Analysis of material instabilities in inelastic solids by incremental energy minimization and relaxation methods: Evolving deformation microstructures in finite plasticity. J. Mech. Phys. Solids 52, 2725–2769.
Miehe, C., Mauthe, S., Hildebrand, F., 2014. Variational gradient plasticity at finite strains. Part III: Local–global updates and regularization techniques in multi-plicative plasticity for single crystals. Comp. Meth. Appl. Mech. Engng. 268, 735–762.
Morrey, Jr., C.B., 1952. Quasi-convexity and the lower semicontinuity of multiple integrals. Pac. J. Math. 2, 25–53.
Ortiz, M., Repetto, E.A., 1999. Nonconvex energy minimization and dislocation structures in ductile single crystals. J. Mech. Phys. Solids 47, 286–351.
Ortiz, M., Repetto, E.A., Stainier, L., 2000. A theory of subgrain dislocation structures. J. Mech. Phys. Solids 48, 2077–2114.
Peirce, D., Asaro, R.J., Needleman, A., 1982. An analysis of nonuniform and localized deformation in ductile single crystals. Acta Metall. 30, 1087–1119.
Peirce, D., Asaro, R.J., Needleman, A., 1983. Material rate dependence and localized deformation in crystalline solids. Acta Metall. 31, 1951–1976.
Petryk, H., 1982. A consistent energy approach to defining stability of plastic deformation processes. In: Schroeder, F.H. (Ed.), IUTAM Symposium on Stability in the Mechanics of Continua. Nümbrecht, 1981, Springer, Berlin, pp. 262–272.
Petryk, H., 1992. Material instability and strain-rate discountinuties in incrementally nonlinear continua. J. Mech. Phys. Solids 40, 1227–1250.
Petryk, H., 2000. General conditions for uniqueness in materials with multiple mechanisms of inelastic deformation. J. Mech. Phys. Solids 48, 367–396.
Petryk, H., 2003. Incremental energy minimization in dissipative solids. C. R. Mecanique 331, 469–474.
Petryk, H., 2005. Thermodynamic conditions for stability in materials with rate-independent dissipation. Philos. Trans. R. Soc. Lond. A Math. Phys. Eng. Sci. 363, 2479–2515.
Petryk, H., 2020. A quasi-extremal energy principle for non-potential problems in rate-independent plasticity. J. Mech. Phys. Solids 136, 103691.
Petryk, H., Kursa, M., 2013. The energy criterion for deformation banding in ductile single crystals. J. Mech. Phys. Solids 61, 1854–1875.
Petryk, H., Kursa, M., 2015. Incremental work minimization algorithm for rate-independent plasticity of single crystals. Int. J. Num. Meth. Engng. 104, 157–184.
Petryk, H., Kursa, M., 2022. Crystal plasticity algorithm based on the quasi-extremal energy principle. Int. J. Num. Meth. Engng. 123, 3285–3316.
Phalke, V., Forest, S., Chang, H.J., Roos, A., 2022. Adiabatic shear banding in FCC metallic single and poly-crystals using a micromorphic crystal plasticity approach. Mech. Mater. 169, 104288.
Po, G., Huang, Y., Ghoniem, N., 2019. A continuum dislocation-based model of wedge microindentation of single crystals. Int. J. Plast. 114, 72–86.
Prüger, S., Kiefer, B., 2020. A comparative study of integration algorithms for finite single crystal (visco-)plasticity. Int. J. Mech. Sci. 180, 105740.
Raabe, D., Roters, F., 2004. Using texture components in crystal plasticity finite element simulations. Int. J. Plast. 20, 339–361.
Reddy, B., 2013. Some theoretical and computational aspects of single-crystal strain-gradient plasticity. ZAMM - J. Appl. Math. Mech. Z. Angew. Math. Mech. 93, 844–867.
Reddy, B., Steinmann, P., Kergaßner, A., 2021. A thermodynamically consistent theory of stress-gradient plasticity. J. Mech. Phys. Solids 147, 104266.

Rice, J.R., 1971. Inelastic constitutive relations for solids: An internal-variable theroy and its application to metal plasticity. J. Mech. Phys. Solids 19, 433–455.

Rice, J.R., 1977. The localization of plastic deformation. In: Koiter, W.T. (Ed.), Proceedings of the 14th International Congress on Theoretical and Applied Mechanics. Delft, 1976, North-Holland, Amsterdam, pp. 207–220.

Roters, F., Eisenlohr, P., Hantcherli, L., Tjahjanto, D.D., Bieler, T.R., Raabe, D., 2010. Overview of constitutive laws, kinematics, homogenization and multiscale methods in crystal plasticity finite-element modeling: Theory, experiments, applications. Acta Mater 58, 1152–1211.

Scheunemann, L., Nigro, P., Schröder, J., Pimenta, P., 2020. A novel algorithm for rate independent small strain crystal plasticity based on the infeasible primal–dual interior point method. Int. J. Plast. 124, 1–19.

Simmons, G., Wang, H., 1971. Single Crystal Elastic Constants and Calculated Aggregate Properties: A Handbook, second ed. M.I.T. Press, Cambridge.

Svendsen, B., Bargmann, S., 2010. On the continuum thermodynamic rate variational formulation of models for extended crystal plasticity at large deformation. J. Mech. Phys. Solids 58, 1253–1271.

Taylor, G.I., 1938a. Analysis of plastic strain in a cubic crystal. In: Lessels, J.M. (Ed.), Stephen Timoshenko 60th Anniversary Volume. Macmillan, New York, pp. 218–224.

Taylor, G.I., 1938b. Plastic strain in metals. J. Inst. Metals 62, 307–324.

Ulloa, J., Alessi, R., Wambacq, J., Degrande, G., François, S., 2021. On the variational modeling of non-associative plasticity. Int. J. Sol. Struct. 217-218, 272–296.

Wang, D., Diehl, M., Roters, F., Raabe, D., 2018. On the role of the collinear dislocation interaction in deformation patterning and laminate formation in single crystal plasticity. Mech. Mater. 125, 70–79.

Wert, J.A., Huang, X., Inoko, F., 2003. Deformation bands in a [110] aluminium single crystal strained in tension. Proc. R. Soc. Lond. Ser. A Math. Phys. Eng. Sci. 459, 85–108.

Yalçinkaya, T., Brekelmans, W., Geers, M., 2012. Non-convex rate dependent strain gradient crystal plasticity and deformation patterning. Int. J. Solids Struct. 49, 2625–2636.

Zhang, M., Nguyen, K., Segurado, J., Montáns, F.J., 2021. A multiplicative finite strain crystal plasticity formulation based on additive elastic corrector rates: Theory and numerical implementation. Int. J. Plast. 137, 102899.